Electric Gradient Field Applied to Lipid Monolayers

A Master thesis by

Asger Tønnesen

Niels Bohr Institute, University of Copenhagen, Denmark

Supervisor
Prof. Thomas Heimburg

Biomembrane Biophysics Group at the
Niels Bohr Institute, University of Copenhagen, Denmark

December 1, 2008

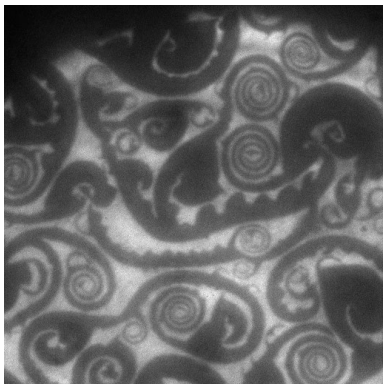

Fig. 1: Art appears in non equilibrium. Fast compression of a DPPC monolayer into the coexistence region between liquid and solid.

Acknowledgement

I wish to thank all the members of our Biomembrane Biophysics Group at the Niels Bohr Institute, especially K. Sigmundson for his encouraging stimulation and comments, A. Blicher for discussions and optimism. M. Gudman for having designed and build the combined Langmuir trough and fluorescence microscopy setup at Niels Bohr Institute and introduced me to the technique. Thanks to the electronic department and the workshop

Without my supervisor T. Heimburg and his innovatory theory and ideas of propagation of impulses in nerves I would not have explored this field. His door was $\approx$ always open.

List of Symbols and Notation

List of general terms and notation for chemicals in the thesis. Materials for the experimental part are listed in Materials and Methods Chapter 5.

Terms

Symbol	Name
d_0	Distance from monolayer to top electrode
DSC	Differential Scanning Calorimeter
E	Electric field applied to monolayer
e.g.	For example (latin: exempli gratia)
G	Energy of a dipole in a electric field
i.e.	That is (latin: id est)
NA	Numerical aperture (of a microscope objective)
MLVs	Multi lamellar vesicles
MMA	Mean Molecular Area ($\AA^2$)
Π	Lateral pressure (mN/m)
Ψ_D	Dipole potential of a monolayer (V)
R	Optical resolution (of a microscope objective)
R_0	Radius of equilibrium of induced circular area
T_m	Melting temperature
U	Voltage
WFM	Wide-field microscopy, wide-field fluorescence microscopy
WD	Working distance (of a microscope objective)

Chemicals

Symbol	Name
DMPE	1,2-Dimyristoyl-sn-Glycero-3-Phosphatidylethanolamine
DPPC	1,2-Dipalmitoyl-sn-Glycero-3-Phosphocholine
DPPG	1,2-Dopalmitoyl-sn-Dlycero-3-Phosphatidylglycerol
POM	Polyacetal Engineering Polymers, Delrin
PTFE	Poly(tetrafluoroethene), Teflon
TRITC-DHPE	n-(6-Detramethylrhodaminethiocarbamoyl)- 1,2-Dihexadecanoyl-sn-Glycero- 3-Phosphoethanolamine, Triethylammonium salt

Contents

Chapter 1

Introduction

1.1 Motivation and Outline

The question of inspiration for the experimental work in this thesis was originally *"How does electrical stimulation of a nerve affect the main membrane components i.e. the lipids?"* The complete answer to this question is unfortunately not given by this thesis.

In spite of the enormous research on nerves including; nerve signaling, receptor proteins for neurotransmitters and anaesthesia, selective ion channels (proteins) etc. little attention has been paid to the probable influence of electrical stimulation on the *lipids*. However the sparse literature on the subject shows that polar phospholipid monolayers are strongly affected by the presence of an inhomogeneous electric field *[Mohwald1986][Heckl1988]*.

In this thesis the question is approached by studying the effect of an electric gradient field applied onto a model membrane resembled with an artificial lipid monolayer in a Langmuir trough. The monolayers consist of the derivative of lipids, which have the highest mass percentage content of lipids in non-myelinated nerves. These lipids are the Diacyl-PhosphatidylCholines (PCs) characterised by polar choline head groups *[Sackmann1995]*. To simplify the model system as much as possible the (1,2-Dipalmitoyl-sn-Glycero-3-Phosphocholine) DPPC was chosen. At room temperature DPPC monolayers can be compressed into any state and have a broad coexistence region containing both a liquid and a condensed phase. This region is relevant in the experimental work, since biological membranes have very broad melting transition profiles and thereby a broad region of coexistence containing phases of the different lipids present in the membranes *[Heimburg2005]*.

Outline of the experimental work:

- Melting properties of DPPC with yhe focus on the important polar head group. Differential scanning calorimetry was used to investigate the influence of the fluprescence marker TRITC-DHPE on multi-lamellar vesicles (MLVs).

- Observations of morphology and thermodynamics of DPPC monolayers at room temperature, which was achieved by using a binary technique of a Langmuir trough combined with wide field fluorescence microscopy (WFM).
- Establishment of a method for stimulation and detection of the effect of an electric gradient field applied to a Langmuir monolayer and conformation of the results from the 1980' by Möhwald and co-workers. A reliable setup for the electricl field was build and designed to fit into the existing setup of a Langmuir trough and the (WFM).
- Performance of additional (and non proceeded) experiments with an applied homogeneous electric field across DPPC monolayers and direct stimulation of DPPC monolayers which are described in Appendix A.1 and A.2.

1.2 Questioning Electro-physiology of Neurons

This thesis will serve as an eye-opener and a brief introduction to what is unexplained about nerve membranes and applied voltage. It is not a defense of schooled theory describing aspects and physiology of nerves. It is widely accepted, that the nerve impulse (signal) propagates along the nerve membrane. The impulses can be measured as electrical analog signals by putting an electrode on the outer membrane and a reference electrode in the environment close to the membrane.

In the human body a variety of nerves exist which can be classified in five groups according to their functions: 1) Motor neurons of spinal cord connected to muscles 2) Sensory neurons widely distributed in the body 3) Pyramidal cells of hippocampus 4) Light sensitive neurons located in the eye retina and 5) Purkinje cells of cerebellum. A typical multipolar nerve cell is illustrated in *fig. 1.1*. It has four morphological regions: the cell body, dendrites, the axon and the pre-synaptic terminals *[Kandel2000]*. Part of the nerves in the human body are piecewise insulated by Schwann cells, which wrap a layer of myelin around the axon. On the micrograph the cross section of a immobilized axon shows the relative dimensions of the myelin layer, the cytoplasm and the impulse conducting cell membrane of the axon. At the nodes of Ranvier between the Schwann cells, direct stimulation and recording of nerve impulses are possible *[Tasaki1939]*. Conduction of the impulse was first modeled by Hodgkin and Huxley in 1952 based on successive influx and efflux of sodium and potassium across the nerve membrane through ion selective channels *[Hodgkin1952]*.

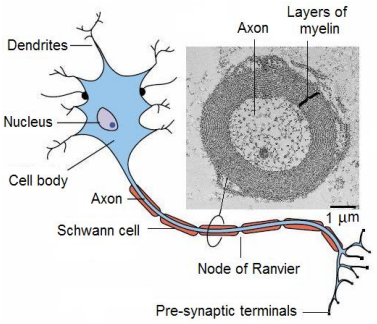

Fig. 1.1: Schematic of a nerve with definitions. The membrane of the axon conducts neuronal impulses. ***Insert:*** *Electron micrograph of nerve cell axon wrapped in myelin from a Schwann cell. Adapted from [Napolitano1967]*

With regards to this model, however, a consequence of the ion currents across the membrane has to be an irreversible production of heat. Beside the electric impulse nerves express a local thermal response and thickening of the nerve which both are in phase

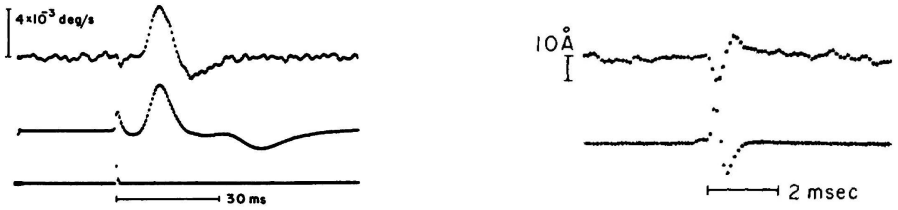

Fig. 1.2: ***Left:*** *(Top trace) Thermal responds of the non-myelinated garfish olfactory nerve in phase with the (lower trace) recorded electric impulse measured at the same point. Adapted from [Tasaki1989]* ***Right:*** *The non-myelinated giant squid axon is thickened by* $0.5\mathring{A}$ *and (top trace) at the same point where the recorded electrical impulse pass. (lower trace). Adapted from [Tasaki1980]*

with the electrical signal. The magnitudes of the two signals made it difficult to detect and first in 1958 - 1960 Abbott managed to setup a heat sensor of the required accuracy. This and following experimental results were considerably different from the predicted heat production by ion fluxes. At the raise of the impulse, heat was released from the nerve but absorbed again in an equal amount *[Abbott1960].* Experiments like these have been performed mainly by Tasaki and co., who worked on both myelinated nerves and non-myelinated nerves, *fig. 1.2 [Tasaki1989] [Tasaki1992].* In 1980 a mechanical swelling of a nerve was detected to have a displacement of the nerve cross section in the order of $0.5\mathring{A}$, and this effect was found in a variety of animals *[Tasaki1980] [Tasaki1989] [Tasaki1999].*

The results imply an electro-mechanical coupling of the compounds in a nerve membrane, neither the thermal response nor the swelling can be deduced from the Hodgkin-Huxley model. If the selective ion channels cannot explain these two detectable effects, logic claims that, the rest of the membrane i.e. the lipids must be involved and therefor be examined. However, the questioning of electro-physiology shows the relevance to the initial question *How does electrical stimulation of a nerve affect the main membrane components - the lipids?* The thermal-mechanical coupling has been approached in *[Heimburg2005]* by introducing a mechanical wave (a soliton) in the lipid membrane and include the melting transition of the membrane. During the melting transition lipid membranes display changes in volume, heat capacity and area compressibility. The mechanical wave pushes the liquid membrane about 85% into the transition.

1.3 Ordered Phosphorlipid Monolayers on aqueous subphase

The distribution of lipid species in nerve membranes wary from nerve to nerve but for non-myelinated nerves, the main part is composed of phospholipids with head groups carrying a charge or has a dipole moment. As an example, the distribution of lipids in a brain nerve from a rat is given in mass percentage, *fig. 1.3 [Sackmann1995].*

Monolayers composed of oily substances on water have been reported since the ancient

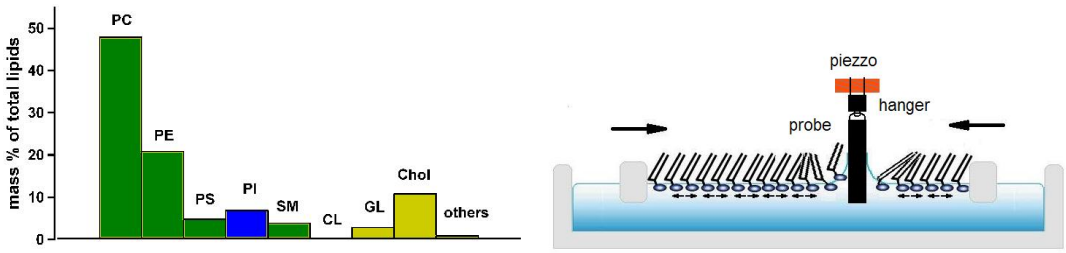

Fig. 1.3: ***Left:*** *Distribution of nerve lipids from the brain of a rat in mass percentage. Green color for lipid with polar head group. Blue is negative charged and yellow for nonionic lipids. Data from [Sackmann1995].* ***Right:*** *Formation of a monolayer after spreading of the lipids and evaporation of the solvent. Hydrophilic head groups orient in the water and hydrophobic carbon chains point away from the water. A probe connected to a piezo crystal is used to convert tension of monolayer-water interface into a voltage difference.*

world by the Pliny the Elder † 79 AD[1] mainly for the reason that a layer of oil damps disturbances of water. In modern time the phenomena was observed by Benjamin Franklin 1774, who noticed that a teaspoon of oil covered an area of several square yards, but he did not calculated the thickness of his film. In 1891 a technique was developed by a young German lady Agnes Pockels. She constructed a ring tensiometer and a trough filled with water. The trough had movable barriers to alter the area and she obtained reproducible experiments of the extension of films and surface tension *[Pockels1891]*. She continued the research in cooperation with Lord Rayleigh, and thus led to his conclusion that a film of amphiphilic acid was only one molecule thick *[Rayleigh1889]*.

Nevertheless, the technique is named after the American scientist Irving Langmuir, who gave a modern molecular understanding of monolayers and pointed out that the amphiohilic molecules showed a preferable orientation due to the "active group" head group of the molecule. Ordering of such molecules are illustrated in *fig. 1.3* right. He also stated from own experiments that spreading follows the 2-dimensional gas law and that palmitic acids and higher fatty acids exerts lateral pressure in the expanded state of the film. From this he concluded the existence of a gaseous phase beyond the solid and liquid phases *[Langmuir1917]*. He and his assistant Katharin Blodgett developed the techniques for transferring monolayers to solid substrates called the LB method *[Blodgett1934]*. Nowadays much attention has been paid to the LB technique, because it facilitates visualization and probing of association phenomena between biological molecules. One should have in mind that membranes on a substrate are immobilized with lack a of kinetics and do not resembles in vivo membranes.

Since the improvements and the conceptual development of monolayer troughs by Langmuir the technique has been intensively used to measure surface properties of all kinds of hydro colloids. Especially, lipid monolayers at the air-water interfaces have been successfully used as models to proximate the behavior of the cellular lipid bilayers, enabling observation of thermodynamical aspects, such as lateral pressure, surface and dipole poten-

[1] 1 Roman naturalist, collected all known science in the book *Naturalis Historia*

tials of Lipid monolayers [Vogel1988] [Brockman1994]. The ingenious design of an inverted microscope combined with a Langmuir trough in the early 1980' enabled direct observations of monolayers with the use of fluorescence markers in monolayers *[VonTscharner1981] [Losche1983] [Loesche1984].* A wide spread research on the subject has since then acelrated. This includes diffusion of lipids and proteins [Saxton1987], the influence of large ions and anaesthesia on lipid monolayers.

1.4 Previous Studies with Electrical Fields Applied to Monolayers

The first scientific results on the subject originates from 1986 published by Möhwald and Miller. Using of a combined setup of fluorescence microscopy and an electric gradient field sketched in *fig. 1.4*, they induced movement of lipid domains in monolayers in the coexistence phase. In the monolayer plane, the equipotential of the field was centered beneath the top electrode. This enabled a control of attraction for at negative charged top electrode (U=-100V) and repulsion of lipid domains for the opposite (U=100V). In the case of attraction, a nearly circular cluster of domains was formed, while a domain empty area of same size was induced for a repulsive field. This was observed for monolayers made of the polar lipids DLPE[2], DMPE[3] and DMPA[4] at pH 11 with the use of fields of strength $5 \cdot 10^6$V/m. With the use of a steel ring held 10μm above the monolayer instead of the electrode, DMPE domains were observed to melt with a field strength of $1 \cdot 10^7$V/m *[Mohwald1986].* They hardly stressed the sign of the charged electrode (the direction of the field), which is opposite to what one should expect for the direction of the domain movement if the polar head groups accounts for the dipole moment of the domains. Beside this contradiction they estimated that a higher density of domains in a cluster was possible relative to domain repulsion.

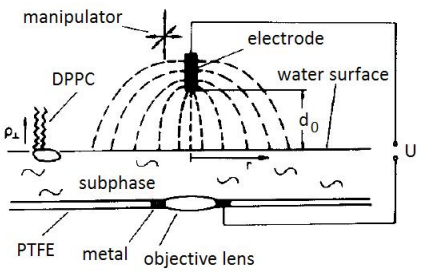

Fig. 1.4: Schematic of the setup for generating a radial electric gradient field at the air-water interface i.e. the monolayer region [Heckl1988]. This setup was of great inspiration for the approach in this thesis.

With a similar setup the group extended the research to include induced movement of domains in monolayers made of DPPC. Two main conclusions arived from these experiments: (1) The direction of the movement depends on the direction of the electric field; (2) The difference of the dipole components normal to the monolayer of the domains and liquid lipids phases, dominates the effect *[Heckl1988].* Thus only the domains are affected by the field. For quantification they obtained that the growth rate of a cluster with a constant voltage decreased with time and assumed that the electric gradient force was

[2] 1,2-Dilauroyl-sn-Glycero-3-Phosphoethanolamine
[3] 1,2-Dimyristoyl-sn-Glycero-3-Phosphoethanolamine
[4] 1,2-Dimyristoyl-sn-Glycero-3-Phosphate (Monosodium Salt)

counteracted by a convective force (drift) in the monolayer. At equilibrium between the forces they defined an radius R_0. It appeared that the voltage applied to the top electrode was proportional to the radius squared, $U \propto R_0^2$. They argued that the force produced by the electric gradient field, for that electrode conformation, was best described with a thin rod approximation *[Heckl1988]*.

However, as they pointed out in their discussion convective forces cannot balance the electric gradient force on the whole parameter of the created circular area. Drift in monolayers has very often a particular direction giving the induced area a convex curve in its slipstream. For strong drift this convex curve is extended and a "tail" of the area is formed. This was actually observed in the first experiments of this thesis and is illustrated in Sec. 6.2. They left an open question about why the domain free and the domains condensed areas are almost circular?

Since the field used has circular equipotentials with the electrode in the center, the question might be answered if repulsion between the domains is taken into account. Because the repulsive dipole forces between the domains in the cluster will superimpose to a resulting dipole force that pointing radial from the center and perpendicular to the equipotentials in the monolayer plane, a circular shape of the cluster is favored. A true description the of two components of the dipoles has not been estimated and is yet not known. It is known from dipole potential measurements that the normal component increases during compression i.e. condensation of the DPPC monolayers *[Vogel1988]*.

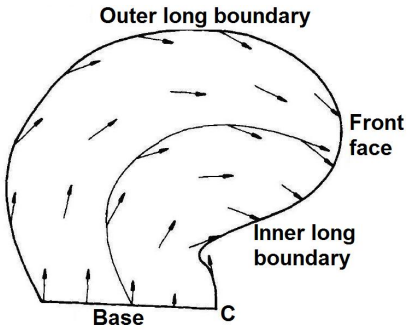

Fig. 1.5: Dipole moments of a domain parallel to the monolayer indicated by arrows. The normal dipole components are strongest at the base and decrease toward the front. Modified from [Florsheimer1989].

In the work from 1989 by Flörsheimer and Möhwald information about the lipid arrangement was obtained by studying fusion and fission processes of lipid domains in a monolayer of DPPC compressed into the coexistence region. Development of domain shapes was observed, when removing the neighbor domains at the same time *[Florsheimer1989]*. Having four electrodes configured in a triangle and one in its median installed 30μm above the monolayer, manipulation of domains was fairly simple. For capturing a domain the potential of two electrodes on the triangle was switched to repel domains. Driven by convection, a domain moved toward the area beneath the median electrode. The potential of the third electrode in the triangle was then switched to keep other domains out of the center area and the central electrode was then charged to keep the domain trapped. Even without increasing the surface pressure and having the temperature between 17-20^oC, growth of trapped domains was observed. Such growth could result in fusion of domains or fission, when an arm developing from domains gets thicker and separates from the mother domain. Controlled rotation of DPPC domains was carried out which implies a non-uniform distribution of the normal dipole component. From observations of fusion and fission (repulsion) of trapped DPPC domains Flörsheimer and Möhwald sketched a possible distribution of dipole moments in a bean shaped domain *fig. 1.5*. Fusion between two domains was only observed when contact was made between

faces and/or outer long boundaries.

Using the knowledge and the triangle-setup described right above they succeeded in controlled growth and fusion of lipid domains using DMPE at 20^oC *[Florsheimer1990]*. These domains differ from DPPC by forming circular domains under normal conditions without development of arms from the domains. This implies a more uniform distribution of the dipoles contained and has to be explained by the shorter hydrocarbon chains and the smaller head group of DMPE *[Mohwald1999]*. Fusion was only possible if the domains touch each other at special spots on their borderlines.

Their main conclusions from DMPE domains are:

1. Collisions of domains do not lead to fusion, normally.
2. When a linkage of two domains at the contact spots occurs, the linkage grow in size and develops a neck-like connection.
3. A complete fusion of two domains takes 1 hour and results in a circular domain.
4. Reversibility of fused domains is not observed. Not even during a little expansion of the monolayer.

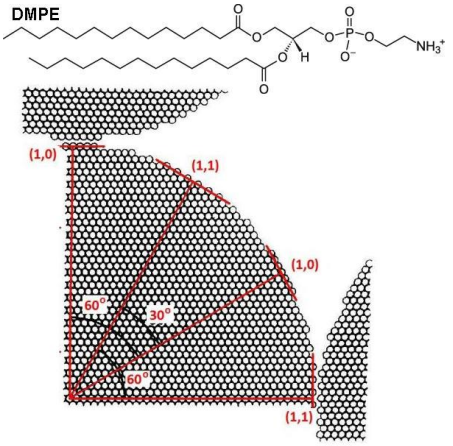

Fig. 1.6: Structure of DMPE and domain fusion which is most probable at spots of equal indices favoring maximal contact of hydrocarbon chains [Florsheimer1990].

They concluded that fusion is most probable when maximal contact between hydrocarbon chains of two circular domains is obtained. They sketched such a situation in *fig. 1.6*, which is provided for hexagonal packing of the domain. They purpose that at maximal contact, attracting Van der Waals forces between the hydrocarbon chains exceeds the repulsion of the dipole forces.

Following these pioneers the technique has been used to measure the behavior of monolayers composed of lipid mixtures. McConnell and co-workers 1995 induced phase separation of the binary mixture DMPC and Dihydrated Cholesterol (now DChol) *[McConnel1995]*. This was carried out for constant temperature, and induced phase separation was measured at lateral pressures above the critical mixing pressure. The experimental setup was different by having a glass insulated electrode sticking through the monolayer, *fig. 1.7*. This also avoided problems with accurate measuring of the *distance* between the top electrode and monolayer. In previous studies as those described above two already co-existing phases were manipulated (i.e. liquid and condensed) but in this study a well mixed phase

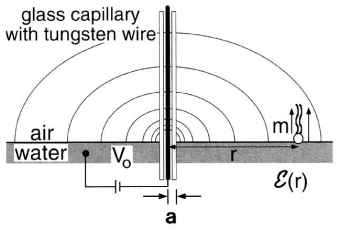

Fig. 1.7: An electric potential is applied to an insulated tungsten wire creating a electric gradient field at the air-water interface, a=6μm. Adapted from [McConnel1995].

containing the non-ionic DChol and the zwitterionic DMPC was separated. Such induced phase separation with an electric gradient field is exclusively due to the difference in dipole moment density between the DMPC and DChol. The dipole moment at the end of DChol made up by the OH group is negligible.

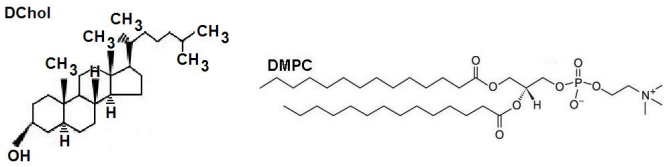

Fig. 1.8: Structure of Cholesterol and DMPC.

A similar effect of a gradient field was observed by Wilke et.al. for the lipid mixture Bovine brain sphingomyelin (Sm) and Ceramide (Cer) in ratios of 9:1 and 8:2. The electrode setup was similar to that of Möhwald 1986-1988 with a single top electrode of diameter 30μm held a distance of 200μm above the monolayer and another in the subphase. With a mix of 90% (Sm) and 10% (Cer) and 145mM NaCl in the subphase the co-existing phases was totally repelled from the region beneath the top electrode with a negatve potential +300V applied to the top electrode. By reversing polarity and thereby the field the two phases clustered in a circular shape, see *fig. 1.9 [Wilke2006a].*

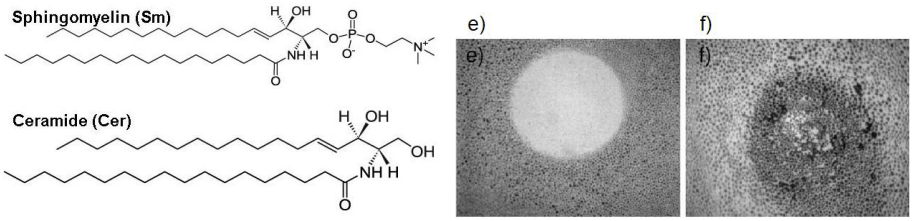

*Fig. 1.9: Repulsion (**left:**) Structure of Sphingomyelin with a polar ethanolamine head group and Ceramide. **right:** In coexistence of 90% Sm and 10 Cer. **e)** Reported repulsion of both phases with +300V applied to the top electrode, **f)** -300V causes attraction and increases of lipid density. Image size 650 × 520μm addapted from [Wilke2006a].*

In the same year, this group published a model for the system based on the electric gradient force and the difference between the dipole densities of the used binary mixtures *[Wilke2006].* They were able to explain the proportionality of applied voltage and radius of induced area $U \propto R_0^2$. The new model failed at low electric potentials, nevertheless the model predicted a threshold value for the electrical potential U for inducing a kinetic movement of the lipids. This value was 100V i.e. $5{\cdot}10^5$V/m for the used setup. In the same work it was experimentally showed that mixtures of (DMPC:DSPC), (DLPC:DSPC) followed the relation $U \propto R_0^2$, which within experimental uncertainty have the same coefficient of proportionality. The size of the induced areas was reported to be similar if the subphase contained 500mM NaCl instead of the usual 145mM NaCl *[Wilke2006].*

Notice:
The experiments from the Möhwald group with DPPC and that only lipid domains are affected by the electric gradient field. The radius of equilibrium of the two areas is unchanged for high concentration of sodium chloride.

Chapter 2

Phase transitions of DPPC Membranes and the Impact of Polar Headgroups

This chapter introduces melting transition of phospholipids with emphasize on DPPC membranes and the role of polar head group. Calorimetry is used on multi lamellar vesicles (MLVs) to clarify the influence of the fluorophore TRITC-DHPE in incorporated in the vesicles.

2.1 Phase Transitions - Biological Relevance

A phospholipid has one or two hydrophobic hydrocarbon chains mounted on a glycerol backbone at which a hydrophilic phosphate group is attached. This amphiphilic structure makes them self organize if they are surrounded by water in structures that keep the hydrophobic chains away from contact with water. Possible structures are micelles, vesicles, bilayers or if deposited on a water surface a monolayer will form. In general phospholipids constitute the largest part of biological membranes and thereby their functions cannot be neglected in any study of such membranes. Besides the phospholipids hundreds of different lipids are presented in membranes surrounding biological cells. To emphasize the role of the lipids it has been shown that composition of the lipids in biological membranes depends on the temperature during cell growth *[Hazel1979]*. Normally the melting temperature of a cell membrane is below body temperature of the organism it self.. This means that at body temperature the lipids are

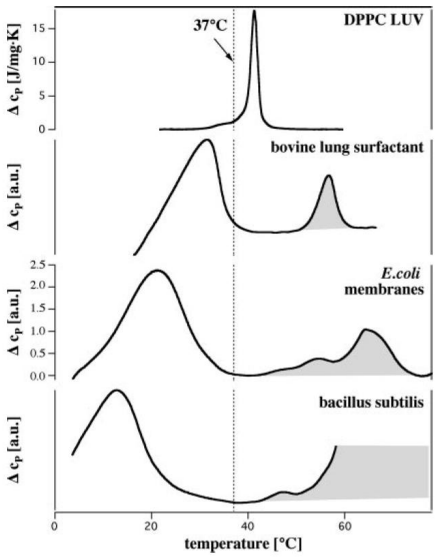

Fig. 2.1: Heat capacity profile which peaks indicate phase transitions. Unilamellar vesicles of DPPC have a melting temperature at $T \approx 41^0C$. The dotted line indicates the body temperature of bovine lung surfactant and growth temperature of E. coli and B. subtilis. Addapted from [Heimburg2005].

melted i.e. the liquid phase. As an example of that *fig. 2.1* provides profiles for measured heat uptake during controlled heating of DPPC vesicles, and cell membranes extracted from bovine lung surfactant, *E.coli* and *B.subtilis [Heimburg2005].*

By decreasing the temperature of a phospholipid membrane below melting temperature of the lipids the membrane undergoes transitions i.e. physical changes into an ordered dense packed state with energy and entropy lower than the liquid state. When the temperature is decreased the lipids pass through four different states as illustrated in fig. 2.2.

- L_α Lipid carbon chains are disordered (fluid) and the lateral order of lipids is random (liquid). Therefore, this phase is also called the liquid-disordered or fluid phase.
- P'_β The lipids occupy partially solid and fluid states with a periodic super structure (ripple-phase).
- L_β Lipids are all in the solid state and 2D crystalline molecular order occurs in the membrane plane. Chains are *all-trans* (ordered) and tilted. This phase is sometimes called solid ordered or gel phase.
- L_C Lipids are all in a 3D crystalline phase.

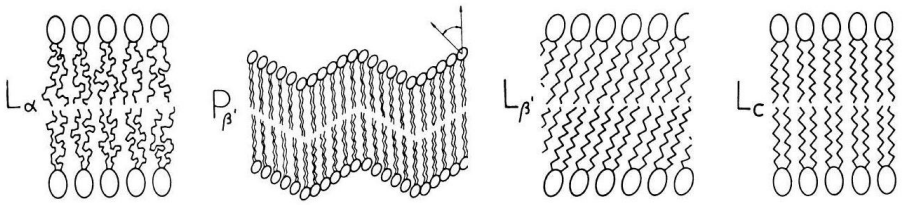

Fig. 2.2: States of a phospholipid membrane during condensation from the liquid state to crystallization. A membrane of DPPC decreases its area by 24% *and increases its thickness by* 16%. *Figure adapted from [Sackmann1995]*

For a particular lipid, transitions between these four states take place at well defined temperatures. Such a transition temperature depends on the intrinsic lipid structure and environmental factors. Longer carbon chains result in higher melting temperature which increases approximately by 10^oC per carbon atom. On the other hand the melting temperature decreases with the number of double carbon bonds, C=C. The influence by the hydrophilic head group is more complicated but increased electrostatic repulsion between charged head groups lowers the melting temperature.

Environmental factors include binding of molecules, ions also H^+ to the head groups. Mixing the membrane with secondary lipids or molecules, especially anesthetics, such as chloroform octanol, ethanol or curare changes the phase transition.

The conformation of carbon chains then depends on the state of the lipid and can change by rotation of the C-C bonds from *gauge* to *trans*. In the gel, a crystalline state, they are "all-trans" for which a carbon chain has reached it full extension and reduced its lateral cross sectional area. A membrane of DPPC will then decrease its area by 24% and

increase its thickness by 16% *[Heimburg1998]*

A change in heat dQ at temperature change dT, defines the heat capacity of the system. Under the condition of constant pressure one obtains the heat capacity c_p from the enthalpy $H = E + pV$ and the 1^{st} law $E = Q - pdV$:

$$c_p = \left(\frac{dQ}{dT}\right)_p = \left(\frac{dH}{dT}\right)_p \tag{2.1}$$

Calorimetric measurements on samples like those in *fig. 2.1* show the heat uptake at a given temperature. Then scanning from below T_1 to T_2 above the melting temperature provides the c_p curve. The melting enthalpy can then be found by integrating c_p from T_1 to T_2

$$\Delta H = \int_{T_1}^{T_2} c_p dT \tag{2.2}$$

The melting temperature T_m is defined as the temperature in the melting transition, where the chemical potential of solid and liquid states are equal. Thus, at this point the difference in the Gibbs free energy ΔG of the two states is zero. $\Delta G = G_{Slid} - G_{Liquid} = 0$. The melting entropy is defined as:

$$\Delta G = \Delta H - T_m \Delta S = 0 \rightarrow \Delta S = \frac{\Delta H}{T_m} \tag{2.3}$$

For DPPC $T_m = 41.3^oC$, $\Delta H = 38.1 kJ/mole$ and $\Delta S = 121.2 J/moleK$.

2.2 On the Diacyl-PhosphatidylCholines

The lipid group of Diacyl-PhosphatidylCholines has a polar choline head group and two carbon chains with n carbon atoms. Three repressentative of these are listed with the number of C-atoms and melting temperature:

	$DLPC$	$DMPC$	$DPPC$	$DSPC$
$n(C-atoms)$	12	14	16	18
$T_m(^oC)$	−3.8	23.6	41.3	54.7

The chain length is the overall dominating factor on the melting temperature, thus the melting temperature can be defined statistically from states of the carbon chains i.e. their conformation. A change in conformation happens if a C-C bond rotates toward one of the three most likely orientations defined by the three minima of the rotational energy with dihedral angles of $\pm 120^o$. One of them provides a global minimum defining the *trans* state while the two *gauche* states have equal rotational energies. The energy difference is such that $gauche = trans \cdot 2.5 kJ/mole$.

The melting temperature of a sample between the solid "ground" state (S) and liquid "excited" state (L) is statistically defined by assuming that the access of the states are

equally probable. In the ground state all the C-C bonds are *all-trans* so only one conformation is possible. Thus the entropy of that state is defined as $S_0 = S_0^0 + K_b \ln(1) = S_0^0$. Let γ denote the mean probability of finding one *gauche* conformation in one C-C bond so $(1-\gamma)$ denotes the probability of finding the rest in *trans*. During melting the entropy change due to C-C bonds is then defined:

$$\Delta S_{C-C} = S_0 - S_0^0 = -k_b \sum_i P_i \ln(P_i) = -2 \cdot k_b \frac{\gamma}{2} \ln\left(\frac{\gamma}{2}\right) - k_b(1-\gamma)\ln(1-\gamma) \qquad (2.4)$$

where $P_{gauche+} = P_{gauche-} = \gamma/2$ and $P_{trans} = (1-\gamma)$

For $T \to \infty$, all *trans* and *gauche* states are equally probable so *gauche* states are weighted 2/3, $\gamma = 2/3$ and the entropy change is:

$$\Delta S_{C-C} = -3 \cdot k_b \frac{1}{3} \ln\left(\frac{1}{3}\right) = k_b \ln(3) \quad (2.5)$$

The entropy scales with the system size since it is a function of state, meaning that the entropy of a Diacyl-Phospholipid with 2 carbon chains of each n C-atoms (n-2 bonds) is given as:

$$\Delta S = \Delta S^0 + 2 \cdot (n-2)\Delta S_{C-C} \qquad (2.6)$$

Similar relation can be obtained for all functions of state, so one has the enthalpy:

$$\Delta H = \Delta H^0 + 2 \cdot (n-2)\Delta H_{C-C} \qquad (2.7)$$

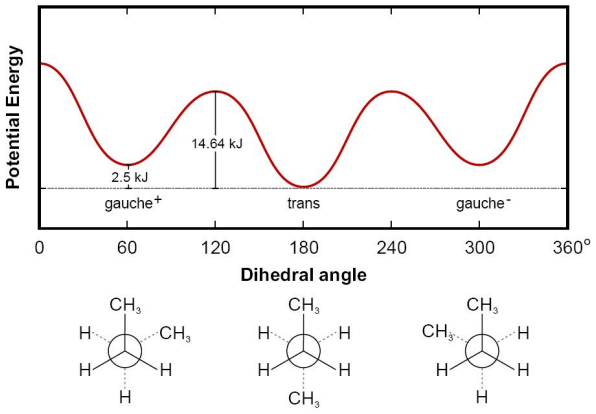

Fig. 2.3: ***Top:*** *Energy landscape of the rotation around a C-C bond. There are three minima one per each 120^o with the lowest energy for the trans conformation.* ***botom:*** *A rotation of the C-C bond from the trans (center) by 120^o results in one of two gauche. Nor rotation direction is preferred due to the energy landscape. Adapted from [Gennis1989]*

The melting temperature is defined where the solid and the liquid state are found with equal probability $P_S(T_m) = P_L(T_m)$ giving a equilibration constant $K(T_m) = 1$.

$$\frac{P_L(T_m)}{P_S(T_m)} = K(T_m) = \exp(-\Delta G/RT_m) = 1 \qquad (2.8)$$

$$\to \Delta G = \Delta H - T_m \Delta S = 0 \to \Delta S = \frac{\Delta H}{T_m} \qquad (2.9)$$

There are two contributions to the total melting enthalpy ΔH of Diacyl-PhosphatidylCholines. One from the melting of the hydrocarbon chains (ch) and one from the polar choline head groups (hg).

$$\Delta H = \Delta H_{ch} + \Delta H_{hg} \qquad (2.10)$$

ΔH_{hg} includes interactions between head groups, such as dipole interactions, Van der Waals interactions, interactions between head groups and the water molecules at the hydration layer and possible hydrogen bonding. ΔH_{ch} is mostly described by the rotational energy and Van der Waals interaction between carbon chains.

With systematic calorimetric measurements of Diacyl-PhosphatidylCholines of different chain lengths n = 12, 14, 16, 18 and 20, the contribution to the melting enthalpy of the head group is recovered. It has previous been shown in this lab that both the change in entropy and enthalpy are linear functions of n. Extrapolating these functions to lower chain lengths than n = 10, the melting displays negative values of enthalpy and entropy, which is not possible for any melting, see *fig. 2.4*. These data agree with data found by others *[Mellier1989] [Russel1975]*.

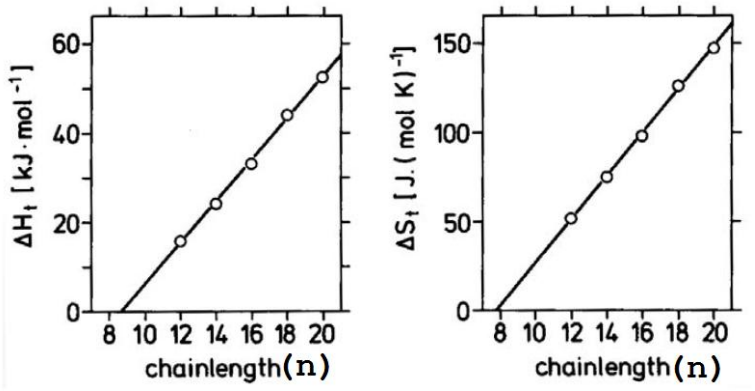

Fig. 2.4: Melting enthalpy and entropy as functions of chain length n are both linear functions. The negative contributions for $n > 10$ stem from change of the head group. Adapted from [Heimburg2007]

Consider the number of C-C bonds the measurements of enthalpy and entropy can be fitted with respect to the number of bonds giving:

$$\Delta H_n = -51.78 + 2(n-2) \cdot 3.20 \frac{kJ}{mol} \tag{2.11}$$

$$\Delta S_n = -134.38 + 2(n-2) \cdot 9.05 \frac{J}{molK} \tag{2.12}$$

for which ΔH_n and $\Delta_s n > 0$ for $n > 10$. It would be a mistake to conclude that a head group and lowest part of the hydrocarbon chains don't undergo changes during the melting transition. Instead the head groups are able to have a more favorable conformation in the liquid than the initial dense packed solid state. For melting of DPPC eq. (2.11) implies that all C-C bonds change conformation corresponding to a melting enthalpy of 89.6kJ/mol and the head group has a negative contribution of -51.8kJ/mol. The corresponding changes of entropy eq. (2.12) are respectively 253.4J/(molK) and -134.38J/(molK). Thus the head groups change conformation during the melting transition and thus should not be neglected in hydrated multilayers or in monolayers on aqueous subphases.

2.3 Influence of TRITC-DHPE on DPPC - Calorimetric Measurements

The fluorescence marker DHPE-TRITC is later used for visualizing the different phases of the Langmuir monolayer in amounts of 0.2mol%. It might influence the structure of the monolayer itself. Deducing the influence of 0.2mol% TRITC-DHPE on the monolayers itself, i.e. change in MMA and lateral pressure, is hardly done from isotherms of the monolayers. The role of air-borne particles contaminating the monolayer was observed to exceed eventually deviations caused by TRITC-DHPE. The strictest evidence for an influence of the fluorophore on a DPPC is if they alter the melting transition of the pure DPPC. Therefore DSC experiments are carried out with multi lamellar vesicles containing the same mole ratio used for monolayers. As mentioned above secondary molecules in a membrane can alter the melting transition.

Materials for DSC scans of MLVs
DPPC was pre-dissolved in ethanol (99% pure) and n-Hexane (5/95 vol%). For the binary mixtures of DPPC and DHPE-RITC, DHPE-TRITC was first dissolved in ethanol (99% pure) to a concentration of 0.2mM and then mixed with pre-dissolved DPPC in the wanted ratio to a final density of 7.4mg/ml. Solvent was evaporated by heating the sample to 35^0C, until a thin film of lipids coated the bottom of the sample glass. The sample was then stored in vacuum over night.

Three scans of the samples were carried out (i) Pure DPPC, (ii) DPPC mixed with 0.2mol% TRITC-DHPE, iii) DPPC mixed with 0.4mol% TRITC-DHPE. Before a scan the vacuumed sample was hydrated in ultra pure milli-Q water to create MLV's. Four heat cooling cycles were carried out $(23 \leftrightarrow 45)^oC$ to ensure hydration of the layers in the vesicles. milli-Q water was used in the reference cell.

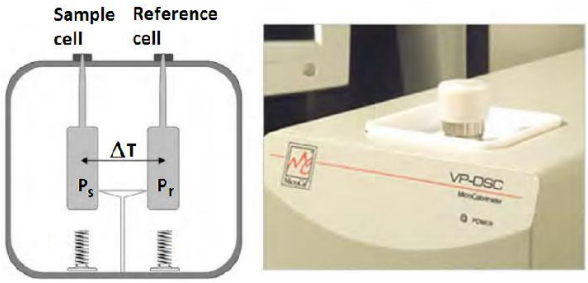

Fig. 2.5: Schematic and of the DSC. The reference cell, sample cell and Peltier heaters P, are isolated with an adiabatic shield. The cells are heated at a constant rate and the temperature difference is kept zero. During the scan the difference in the heating powers ($P_s - P_r$) is recorded as a function of temperature.

The DSC Method
A DSC is made with a reference cell and a sample cell connected with a thermocouple each cell has a heater, see *fig. 2.5*. Starting with the solid lipid sample the essential is to keep the temperature difference between the two cells at zero while slowly changing the

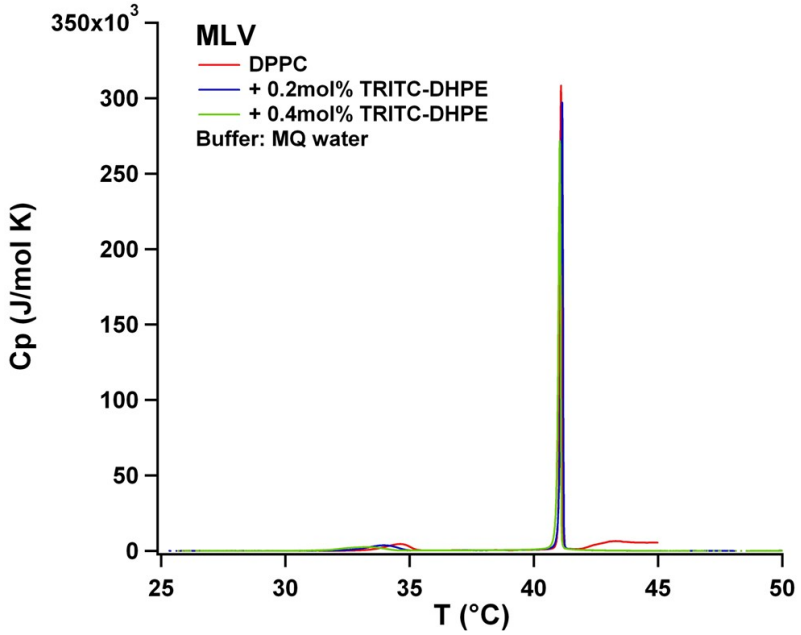

Fig. 2.6: Heat capacity profiles of MLV for pure DPPC and DPPC/TRITC-DHPE mixtures hydrated with milli-Q water.

temperature at a constant scan rate K/s. By heating both cells at constant rate J/s the increased heat uptake of the sample relative to the reference during the phase transition is compensated by heating the reference until the temperature difference is zero. This is recorded as a function of temperature. Dividing the power profile with the scan rate one obtains the heat uptake of the sample per temperature which defines the heat capacity c_p, with units of J/K.

2.4 Conclusion on the influence of TRITC-DHPE

Fig. 2.6 provides the measured heat capacity profiles of MLV for pure DPPC and DPPC/TRITC-DHPE mixtures. For multi lamellar vesicles of DPPC the c_p curve is very narrow around the melting temperature. T_m is then easily defined at the maximum of the Cp curve. The calorimetric scan shows that a pure DPPC (red) has $T_m = 41.1$ which deviates 0.2^oC from the standard value of 41.3^oC *[Heimburg2007] [Biltonen1993]*. For the samples containing 0.2mol% and 0.4mol% fluorophore the melting temperatures are respectively 41.14^oC and 41.08^oC. The fluorophore lovers the main transition peak of the c_p curve and a negligible broadening with the amount of fluorophore is indicated. The unusual shoulder of the c_p curve for pure DPPC after the main melting transition should be noted but remains unexplained. It is then concluded that a use of $0.2mol\%$ TRITC-DHPE has no influence on a DPPC membrane. This amount will be the upper limit for fluorophore concentrations used in the monolayer experiments.

Chapter 3

Isothermal Compression of DPPC Monolayers - Phases and Morphology

This chapter gives an introduction to monolayers made of DPPC and an understanding in advance of the experiments reported in Chapter 6 including electrical manipulation of DPPC monolayers. Relevant thermodynamics of monolayers on aqueous subphases is mentioned parallel with obtained results of isothermal compression of DPPC monolayers. This also includes imaging of the monolayers with the use of the fluorescence microscopy technique.

3.1 Introduction

Ever since the first scientific work with monolayers by Pockels and Rayleigh and the conceptual development by Langmuir, information of phase transitions and phases of monolayers have been gained from isotherms. On that basis, a macroscopic understanding of monolayers based on thermodynamics evolved and is best reviewed by *[Gaines1966] [Langmuir1917]*. However a mesoscopic view of monolayers was first accomplished early in the 80' using fluorescence dyes only soluble in the liquid phase of the monolayers *[VonTscharner1981] [Losche1983] [Loesche1984]*. Improvements of fluorescence microscopy and fluorescence dyes had demonstrated the power of the technique *[Benvegnu1992]*.

The fluorescence marker TRITC attached to DHPE used here is well soluble in the liquid phase of DPPC and allows visualizing of shapes of non-liquid structures like condensed domains and gaseous air-pockets if they co-exist with a liquid phase. The influence of TRITC-DHPE on the lipid-matrix of DPPC is shown in Chapter 2 to be negligible. By compression of a DPPC monolayer from the disordered liquid phase, the lipids condense into flat structures called domains. For the lipids in the domains the two hydrocarbon chains are tilted by 30^o from vertical. Only in the solid phase all the hydrocarbon chains are vertical oriented *[Kjaer1987]*. Possible domain shapes are reported to be bean shaped or having two or more lobes which overtime transform into the bean shape which grow during compression until they occupy the whole monolayer and pack in a hexagonal superlattice [Vanderlick1998]. Phospholipids with smaller head groups like PE's (phos-

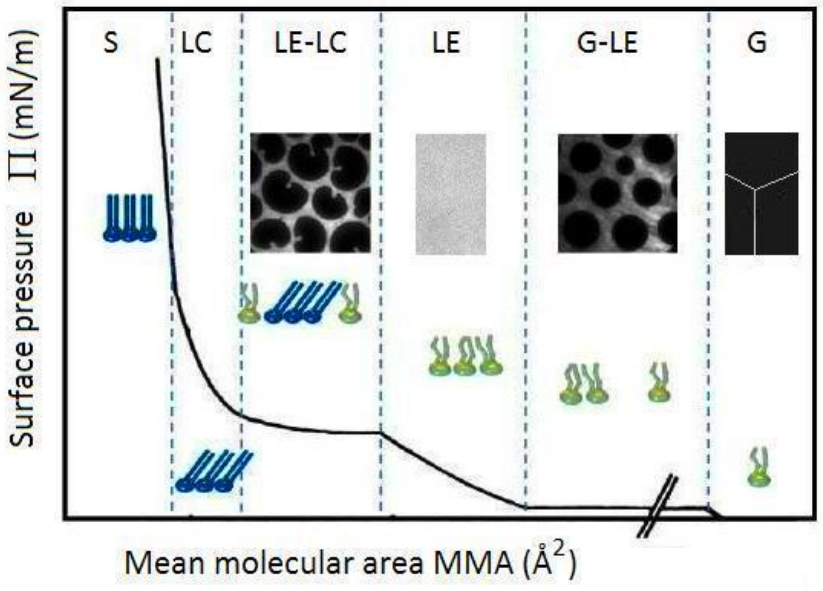

Fig. 3.1: . Idealistic isotherm that outlines the different phases of a DPPC monolayer. Drawings represent the states of the lipids. Inserted images are experimental recordings of the monolayer in that particular phase with an imitated picture for the pure (G) phase. The liquid expanded phase (LE) appears bright because it contains fluorescence. Freshly spread DPPC occupies the gaseous phase (G). There are two regions of coexistence of two phases, (G-LE) and (LE-LC). During compression the monolayer is forced through following phases: the gaseous phase (G), the gaseous and liquid expanded phases (G-LE), the liquid expanded phase (LE), liquid expanded and liquid condensed phases (LE-LC), liquid condensed (LC) and solid phase (S). At a sufficiently critical pressure $\Pi_c > 40mN/m$ the monolayer collapses and fractures of the layer convolute into secondary three-dimensional structures [Volhardt2006]. Modified from [Mohwald1999].

phatidyethanolamine) do not show any tilt and the condensed domains formed are all circular *[Mohwald1999]*.

In equilibrium the shape of a domain is determined by three factors. 1) Internal electrostatic repulsion between the head groups (charged or polar). 2) Molecular chirality of the lipids. 3) Line tension that minimizes the energy difference between liquid and condensed phases hence decrease the circumference of the domain *[Benvegnu1992]*. By using a Langmuir trough, several intensive and extensive parameters can be varied. The intensive variables (i.e. independent of the size of the system) usually measured are: Lateral pressure Π, Temperature T, Surface potential Ψ. The extensive variables (dependent on size of the system) are for monolayers: No. of the i molecules n_i, Area A, Charge or dipole moment p of the molecules q.

The states of the DPPC monolayers investigated in the thesis are defined by the $\Pi - A$ isotherm in which the different phases of a DPPC monolayer are interpreted *[Gaines1966]*. The widely used names and labels of phases are mentioned for convenience starting at the highly expanded pure gaseous state. Gaseous phase (G), gaseous and liquid expanded (G-LE) region, liquid expanded (LE), liquid expanded and liquid condensed (LE-LC) region,

liquid condensed (LC) and solid phase (S). An overview of a isotherm and different phases and lipid states is sketched in *fig. 3.1*.

3.2 Thermodynamics of DPPC Monolayers

Creation of monolayers and the gaseous phase
When spreading a lipid solution on the clean water surface, a wave of expansion is observed. This is an amazing view because it is not the one of a *stone thrown into water*. The wave of expansion arise because each lipid tends to order itself with the hydrophilic head group toward the water and the hydrophobic carbon chains pointing away. This massive ordering gives rise to a wave with direction of expansion toward the clean water surface. The two dimensional lateral pressure of the solvent spread then depends on the art of lipid spread and the area $\tilde{A}$ of the water surface available *[Langmuir1917]*.

To ensure the state of the newly spread monolayer is in the (G-LE) region, the molecule dimensions and trough dimensions should be considered. Neglecting the bend of the water surface at the trough edges the surface area available in this case is $\tilde{A} = 0.15\text{m} \times 0.05\text{m} = 0.0075\text{m}^2$. By assuming the mean molecular area of DPPC to be $50\mathring{A}^2$, an amount of $8 \cdot 10^{-9} mole$ lipids spread requires a surface area of $0.0024m^2$. This is $\frac{1}{3}\tilde{A}$ and results in a mean molecular area of spreading point $150\mathring{A}^2$ well defined in the (G-LE) region.

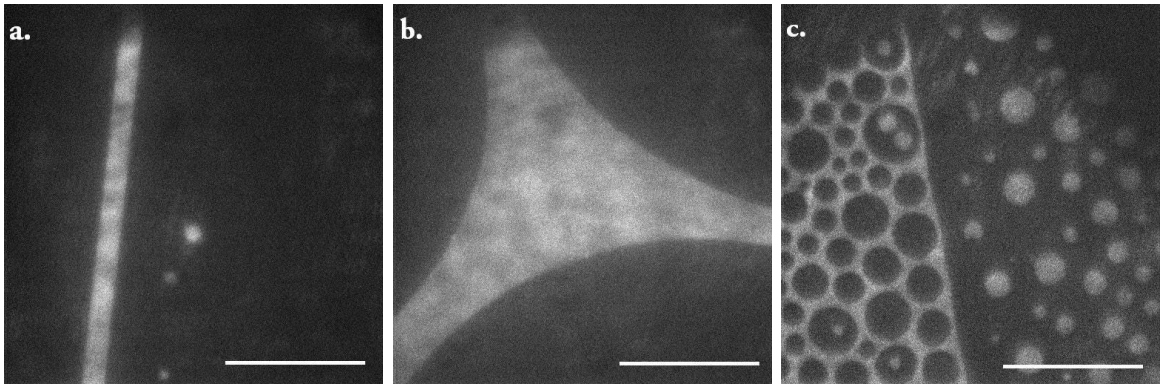

Fig. 3.2: Coexisting of gaseous (G) phase appearing (dark) and liquid expanded (LE) phase (bright) in a DPPC monolayer. **a.** *and* **b.** *are recorded at a MMA of $117\mathring{A}^2$ at different positions.* **c.** *During compression the hexagonal gaseous domains shrinks in size and circular shapes are formed. At a non-defined MMA a phase boundary between (G) and (LE) can be observed.* ***Conditions:*** *Scale bar = $20\mu m$, Mean temperature 22.7^oC, 0.2mol% TRITC-DHPE, Compression Rate $2\mathring{A}^2/molecule/min$.*

Coexistence of the gaseous and liquid expanded phases in the (G-LE) region is illustrated in *fig. 3.2* at a mean molecular area of $117\mathring{A}^2$. The gaseous (G) phase appears dark containing no fluorophore and the liquid expanded (LE) phase is bight because the solubility of the fluorophore in this phase is high. During compression the gas-pockets shrink and disappear at the transition to the pure (LE) phase. A phase boundary of the two phases is observed upon further compression. This gaseous phase is not investigated further in this work.

The solvent itself and the concentration of the lipids in the solvent have individual influences on the $(\Pi - A)$ isotherm. A lipid concentration around or smaller than 1mM is recommended *[Gaines1966] [Mohwald1998]*. The solvent used for spreading has to be chosen with care to ensure the surface tension of water γ_0 is higher than both that of the solvent $\gamma_{solvent}$ and the interfacial tension between water and solvent $\gamma_{solvent,0}$. This satisfy this relation to be positive:

$$\gamma_0 - (\gamma_{solvent} + \gamma_{solvent,0}) \tag{3.1}$$

If this is negative the solvent will not spread and unwanted lipid structures forms. By this and the importance of fast evaporation of the solvent and the requirement of insolubility with the aqueous subphase, chloroform is often used. Hoverer the use of n-Hexane as solvent give fine results and it is less health damaging. For these reasons it is used as the standard solvent for DPPC monolayer experiments in this work. Physical properties for different candidates of solvents are listed in *fig. 3.3*.

	Melting point °C	Boiling point °C	Solubility in water 25°C (g/100g H_2O)
n-hexane	- 94	69	0.01
cyclohexane	6.5	81	0.07
benzene	5.5	80	1.8
chloroform	- 64	61	8
ethyl ether	- 116	35	75

Fig. 3.3: Solvents historically used to perform monolayers. Low solubility in water and low boiling point are highly wanted properties for obvious reasons Well discussed in [Gaines1966].

Isothermal compression

The lateral pressure Π of the monolayer is defined as the difference between the surface tensions of water γ_0 and the surface tension of monolayer-water γ.

$$\Pi = \gamma_o - \gamma \tag{3.2}$$

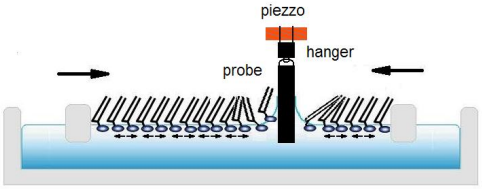

Fig. 3.4: Principle of a Langmuir trough with a balance made of a probe and a piezo crystal that detects the surface tension and convert this into a voltage difference. Isothermal compression increases the surface pressure by reducing the available surface area. (not in scale).

Π increase during compression because of the reduction of γ due to increased repulsion between the lipids. The lateral pressure is detected as the drag on a probe that hangs from a piezo crystal which responds the lateral pressure with a voltage difference. This electronically film balance has an accuracy of 0.1mN/m and had to be calibrated, usually with the known value for pure water $\gamma_0 = 72.8$mN/m at 20^{o}C or a known difference in weights.

The change in the free energy dF of a DPPC monolayer with an applied electrical field E having n lipids with an dipole moment p is given as:

$$dF = -SdT + \mu dn - PdV - \Pi dA + pdE \tag{3.3}$$

This is quickly reduced for a DPPC monolayer with the use of eq. (3.2) to:

$$\Pi = -\left(\frac{dF}{dA}\right)_{T,n,V,q,E} \tag{3.4}$$

which defines the Π-A isotherm. Upon compression, with these conditions, the monolayer undergoes a first-order phase transition from the (LE) to the (LC) phase, corresponding to

a chain ordering *[Pink1982]*. The lateral pressure Π is defined for equilibrated states during the compression but experimental practice implies that this is impossible. In addition, huge experimental experience is needed to have n nearly constant. Used materials and further considerations of the trough are referred to Chapter 5.

The $\Pi - A$ isotherm is plotted as mN/m versus the mean area of one molecule $\AA^2$/molecule. In *fig. 3.5* isotherms are obtained with the setup at different temperatures in the room temperature regime with a subphase of 150mM NaCl. The plateau defining the (LE-LC) coexisting region is chiefly observed. The (LE-LC) region shifts to higher lateral pressure and its width decreases with higher temperatures. At a temperature of 20^oC the boundary coordinates (MMA,Π) of the coexisting phases are approximately ($82\AA$/molecule, 5mN/m) and ($55\AA$/molecule, 10mN/m). It is reported in the literature that the (LE-LC) region for

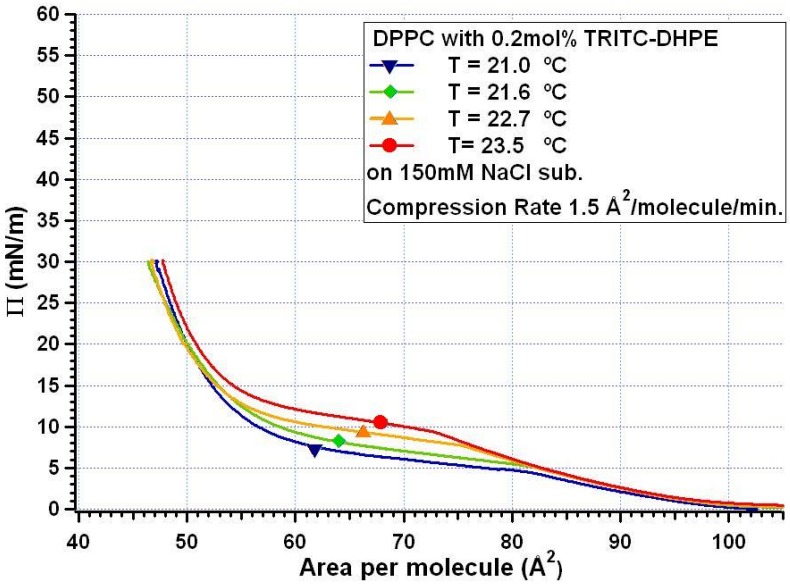

Fig. 3.5: Isotherms of individual DPPC monolayers spread on a $150mM$ sodium chloride subphase are obtained at different room temperatures. The (LE-LLC) phase of interest is expressed at these temperatures. At a temperature of 20^oC the boundary coordinates (MMA, Π) of the coexisting phase are approximately $(82\AA/molecule, 5mN/m)$ and $(55\AA/molecule, 10mN/m)$. ***Conditions:*** *Scale bar = $20\mu m$, subphase of $150mM$ NaCl, 0.2mol% TRITC-DHPE, Compression Rate $1.5\AA^2/molecule/min$, temperatures was stabilized with a heat bath.*

DPPC monolayers shrink for increased temperatures and vanish at a critical temperature of $T_c \approx .40^oC$ *[Mouritsen2007]*.

The lateral compressibility κ_T of the monolayer is a function of molecular area A and lateral pressure Π and is defined as:

$$\kappa_T = \frac{1}{A}\left(\frac{dA}{d\Pi}\right) \tag{3.5}$$

In the (LE-LC) region a small change in lateral pressure results in a large change in the area of the monolayer relatively more than for the other phases. Thus, the compressibility

of a DPPC monolayer has a maximum in the (LE-LC) region where both liquid lipids and condensed domains are presented *[Heimburg2007]*.

3.3 Images of the (LE-LC) coexistence region of DPPC Monolayers

In order to achieve a well illustrated overview of the formation processes of condensed DPPC domains several experiments were carried out with the normal experimental conditions mentioned above and described in Chapter 5. The point of domain formation is

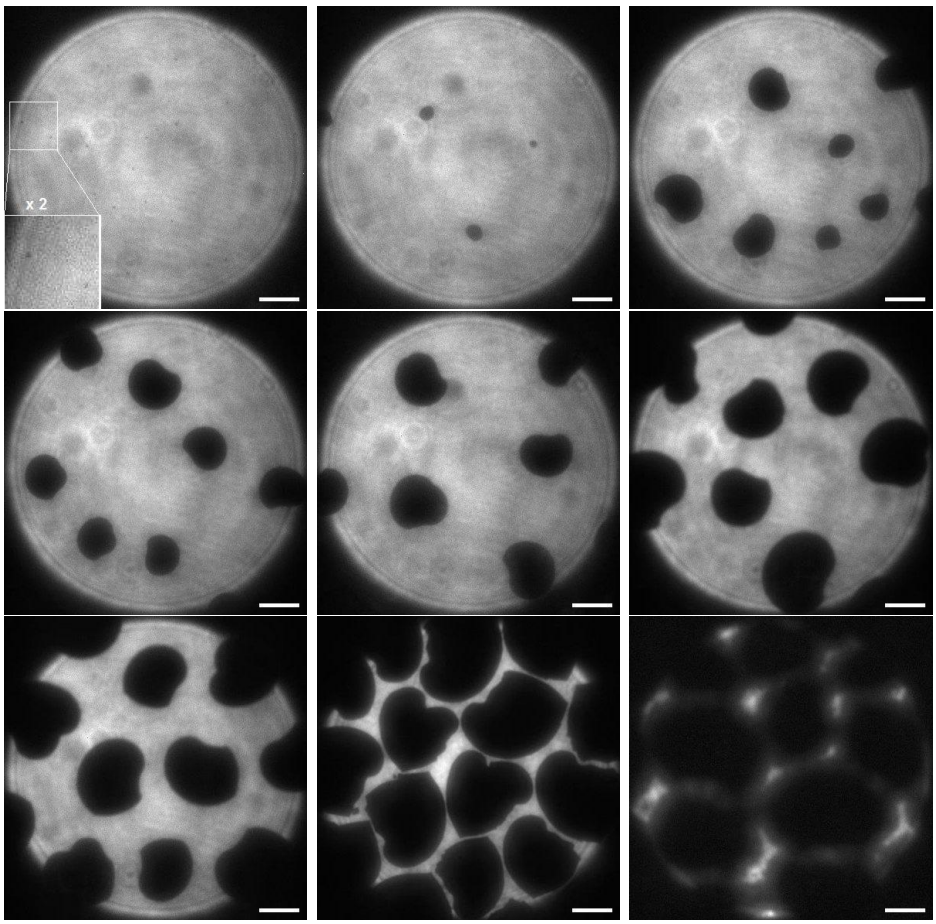

Fig. 3.6: Formation and growth of domains in the (LE-LC) region during an isothermal compression. Domains appear dark while the fluorophore soluble liquid phase appears bright. ***a.-h.*** *Represents the beginning and end of the (LE-LC) region having the first observable domains at the transition about* $80 Å^2/molecule$. ***a.*** *The diameter of the hardly observable micro domains are* $\approx 1\mu m$. *The shape of a domain mainly develops as a bean like shape.* ***i.*** *is recorded at the transition to the (LC) phase where the picture gets blurred.* ***Conditions:*** *Scalebar* $= 20\mu m$, *Mean temperature* 21^oC, *0.2mol% TRITC-DHPE, Compression Rate* $1 Å^2/molecule/min$.

found to be between the (LE) phase and the (LE-LC) region at mean molecular areas

slightly below the kink of the isotherm. As a result of slow compression the domains develops nearly equal in size and shape until the end of the (LE-LC) region, see *fig. 3.6*. The domain shape mainly develops as a bean like shape but round or domains with lobes are also observed. Lobed domains hinder a hexagonal packing of the domains in the (LC) phase but dense packing is always observed. The electrostatic repulsion between domains actually facilitates such packing. Only at high pressures the lattice structure brakes down and the monolayer enters the solid phase (S) in which structures are hardly observable because of the fluorophore do not participate in that phase of the monolayer.

3.4 Conclusion

Isotherms for different temperatures of DPPC monolayers on a subphase of 150mM NaCl are obtained expressing phases and transitions to a fine degree. This includes transitions from (G) to (LE) and from (LE) to (LC) but the transition into (S) hardly determined from the isotherms alone. The dependency of the monolayer on temperature is found to be comparable with literature.

The method of fluorescence microscopy used with TRITC-DHPE is well suitable for obtaining high resolution images of DPPC monolayers except in the (LC) and (S) phases. Shapes and edges of domains are clarified to an accuracy $\approx 1\mu$m similar to the Rayleigh resolution of the optics derived in Chapter 5.

It is found that the rate of compression influences the domain shape, domain size and distribution of the domains in the monolayer. The best results are achieved with slow compression rates. A compression rate of $1.5\mathring{A}^2$/molecule/min. turns out to give reproducible results and is selected as an upper limit for the experiments with applied electric gradient field presented in Chapter 6. The rest of the thesis concentrates on electrodynamic properties of DPPC monolayers interrupted by materials and methods in Chapter 5.

Chapter 4

The Polar Headgroup of DPPC - Origin of Membrane Surface Potential

This chapter treats potentials across membranes with an emphasize on the dipole potential of DPPC monolayers and connect this to the phases of such monolayers.

Biological cell membranes in aqueous environment are from nature a compound of lipids and proteins with lipids as the basis assembled in two co-planar leaflets. Most of the membrane lipids are amphiphilic phospholipids with hydrophilic head groups, charged or polar, and hydrophobic carbon chains directed into the interior of the membrane. This minimizes the contact of the carbon chains with ions, water and other polar molecules in the aqueous environment. Ion concentrations on both sides of the biological membrane and the high densities of charged and polar head groups, separated by a membrane thickness of commonly 5 nm, produce high electrostatic potentials across the membrane. In the literature *[Brockman1994] [Clarke2001]* the potentials are often named as:

1) Transmembrane potential Ψ_C generated by ion gradients across the membrane.

2) Surface potential Ψ_Q arising from fixed charges at the lipid head groups and membrane proteins.

3) Dipole potential Ψ_D of the dipoles at the lipid-water interface.

These are sketched for a bilayer between two aqueous media, *fig. 4.1*:

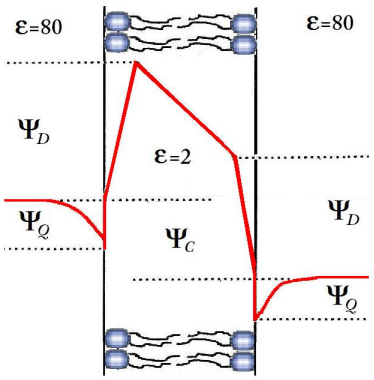

Fig. 4.1: Sketch of potential gradients across a phospholipid bilayer. The transmembrane potential Ψ_C is caused by different concentrations of ions on each side of the membrane. Charged head groups define the surface potential Ψ_Q and dipole potential Ψ_D arises from dipoles present in the bilayer.

The transmembrane potential Ψ_C is of magnitude 10 - 100 mV in biological membranes which facilitates accumulation of proteins on the membrane surface *[Kroon1989]*. It also causes transmembrane movement of ions down their concentration gradients e.g. ions like

Na^{+1}, K^{+1}, Cl^{-1} and Ca^{+2}. An uncountable number of experiments with ion gradients or with a controlled external potential applied across biological membranes have suggested such transport of ions gated through ion selective channels in the membranes. The widely used Patch-Clamp method and single channel analysis in such experiments was developed in 1976 by Neher and Sackmann for which they got the Nobel prize *[Neher1976]*. However ion transport similar to the single channel events is reported to occur across artificial membranes only consisting of the phospholipid DSPC. Maximum of the ion conduction occurs in the melting regime of DSPC ($Tm = 50°C$) *[Antonov1980]*.

The surface potential Ψ_Q of a membrane consisting of 40% negatively charged lipids in a biological environment of a ionic strength of 150mM NaCl has a magnitude about -50 to -100mV *[Heimburg2007]*. The surface potential decays exponentially with the distance from the charged surface and can further be reduced by binding of ions *[Brockman1994] [Heimburg2007]*. Research on the surface potential of both natural and artificial bilayers has mainly focused on its ability to bind ions, proteins and may regulate enzyme activities *[Kroon1989]*.

Since DPPC monolayers are used in this work the dipole potential is treated from now. Dipole potentials Ψ_D of membranes or monolayers arise from the polar head groups on the lipids like the phospholipids PE's, PC's, PS's and Sphingomyelin. For these lipids the dipole moment $\mathbf{p}$ is oriented from the negatively charged phosphate to a positive charged group directed away from the membrane surface. Ψ_D can be measured with the black lipid membrane technique in which two small containers with buffer solution are separated only with an artificial membrane. The basis in such Ψ_D measurement is the rate-constants of transporting large hydrophobic anions and cations across the membrane. It appears that hydrophobic anions are transported across membranes, of typical phospholipids, at rate constants faster than the equivalent cations. Thus, in the center of the membrane Ψ_D must assume positive values relative to the aqueous phase which for DPPC bilayers Ψ_D varies between 200mV and 280mV *[Flewelling1986]*.

Regarding monolayers, the terms Ψ_D and Ψ_Q are mixed into the collective term "surface potential" and what is actually measured depends on the monolayer composition. Measurements of Ψ_D or Ψ_Q requires an electrode in the aqueous subphase and a metal plate in the air above the monolayer. Without a monolayer the potential jumps across the clean water-air interface ψ_w and the potential jumps across the air-metal plate interface ψ_{met}. Connection of the metal plates gives the interfacial potential $\psi_{met} - \psi_w = \Phi$. Thus the reference point, often the water sheet just below the air-water interface, determines the sign of the "surface potential".

An often used technique is the *vibrating plate*. A plate above the monolayer excecutes controlled oscillations which generates an AC current in a circuit because of the potential Φ. By applying a potential Φ' of oppo-

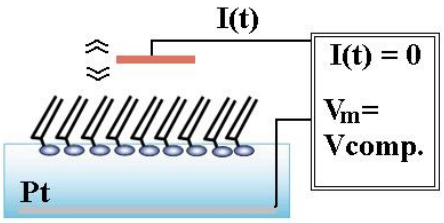

Fig. 4.2: The change of the surface potential V by forming a monolayer can be measured with the condenser method. Periodic vertical oscillation of the plate above the monolayer induce a AC current I(t) which is depressed with a potential V′ to I(t) = 0 at which point V′ equals the membrane potential.

site sign of the potential Φ to the circuit, the AC current is reduced to zero. At this point, Φ is given as Φ'. A calibration by setting the potential to zero for the clean water-air interface ($\psi_{met} = \psi_w$) gives the *surface potential* defined as the difference between the clean water ψ_w and a surface with added lipids ψ_{w+l} is $\psi_{w+l} - \psi_w = \psi_{w+l} - \psi_{met}$. A contribution of ordered water molecules is subtracted by such a calibration *[Brockman1994] [Clarke2001]*. It has been shown that the ordered surface water that causes ψ_w, is estimated to be 100mV *[Palush2002] [Parfenyuk2002]*. The role of water ordering in the head group region is not understood. Attention has to be paid when comparing dipole and surface potentials of a bilayer to monolayer since the potential of a monolayer highly depends on the density of the lipids. Normally one compares measured values of the potentials corresponding to the mean molecular area of the lipids in the monolayer *[Brockman1994]*. For a DPPC monolayer the dipole potential at a mean molecular area of 49$\mathring{A}^2$ is reported to be 500mV to 520mV *[Nakahara2005] [Shapovalov1998] [Vogel1988]*.

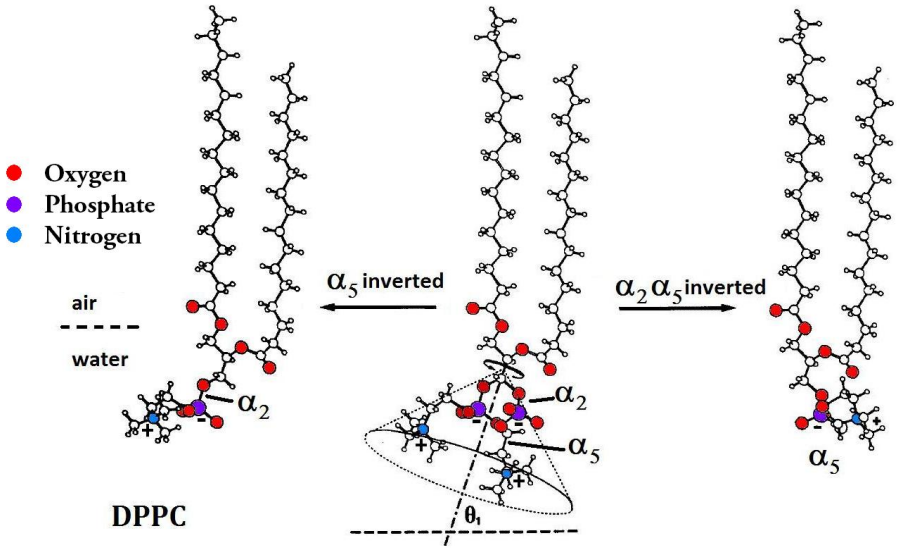

Fig. 4.3: Possible conformational changes of the choline head group on a DPPC molecule. In contact with a water surface the hydrophilic choline will the conformation (middle) since only one rotation enables different orientations. Adapted from [Hauser1981]

4.1 The Head Group of DPPC

From x-ray and neutron diffraction studies of phospholipid multilayers the orientation of a polar headgroups remain approximately parallel oriented to the layer interfaces both in the gel and liquid state for different degrees of hydration. Both DMPC and DPPC shows such a behavior *[Franks1976] [Hauser1981]*. For a DPPC monolayer on aqueous subphase a constant orientation of the headgroups is not the case. However the x-ray studies give information of distances and spaces. The distance between the phosphate and the nitrogen atoms in the choline group is found to be $|P...N| = 4.3$ - $4.5\mathring{A}$ and. The distance is then

assumed to be the same within DPPC giving rise to a dipole moments of DMPC and DPPC defined as pointing from (-) to (+).

The hydrophilic nature f the head groups in a DPPC monolayer ensures that the polar headgroups are oriented toward the subphase. The actual orientation of the choline group and the glycerol backbone in the water depends on the phase of the lipids but a satisfying description is not available. Possible conformations of the headgroup of a DPPC molecule are ginevn in *fig. 4.3*. The most probable configuration allows the headgroup to orient freely on a cone by rotation of one C-C bond *[Hauser1981]*.

Combined measurements of the $\Pi - A$ isotherm simultaneously with surface potential enable a calculation of the average dipole moment normal $p_\perp$ per molecular in a media with a relative permittivity ϵ. For a layer of homogeneously distributed polar molecules on a 2D lattice, the surface potential Ψ_D is described with the Helmholtz equation:

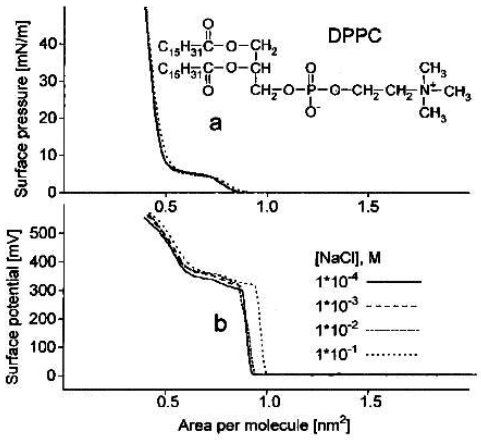

Fig. 4.4: DPPC isotherm (a) and dipole potential (b) at 21^oC for different concentrations of sodium chloride. Adapted from [Shapovalov1998].

$$\Psi_D = \frac{p_\perp}{\epsilon_0 \epsilon A} \tag{4.1}$$

A measured value of the dipole potential of a monolayer is an average of all contributions in the detected area. Using e.q. (4.1) to calculate the dipole moment from a measured value of the dipole potential gives an average of dipole components normal to the monolayer.

For a DPPC monolayer compressed to a mean molecular area of $49\mathring{A}^2$ the surface potential assumes $\approx$ 500mV. If it is assumed that the dipole moment is located above the water surface in the air ($\epsilon = 1$) (used by many authors, see *fig. 4.5*) the Helmholtz equation yields $p_\perp = 4.3 \cdot 10^{-30}$Cm = 0.64 Debye[1].

If instead, the dipole moment is exclusively ascribed to the choline head group embedded in water ($\epsilon = 80$) one gets $p_\perp = 51.2$ Debye.

In relation to the large distance between the phosphate and nitrogen, the dipole moment p of two charges $+q$ and $-q$ spanned by a distance $d = 4.2\mathring{A}$ is calculated. For the charges it is assumed $|+q| = |-q| = e = 1.6 \cdot 10^{-19}$C. Thus, the dipole moment of the choline group is:

$$p = qd = 6.7 \cdot 10^{-29} Cm = 20.1 Debye \tag{4.2}$$

Consider a monolayer or bilayer made of DPPC in a state of $49\mathring{A}^2$/molecule surrounded by pure disordered water with $\epsilon = 80$. In the case that the dipoles are oriented normal to the surface one calculates the dipole potential , by using p = 20.1Debye and eq. (4.1) to Ψ_D = 192mV similar to what is measured for bilayers (200 - 280mV) *[Flewelling1986]*.

[1] 1Debye = $3.335 \cdot 10^{-30}$C^{-1}m^{-1}, $\epsilon_0 = 8.85$C^{2}N^{-1}m^{-2}.

The contributions to the dipole potential from the two polar C=O groups on the headgroup are not estimated here. A more precise calculation of the dipole moment of the head group should be based on quantum mechanics and calculation of the polarization due to electron distributions of the nitrogen and phosphate atoms.

4.2 Influence of Temperature and sodium chloride

With parallel measurements of Ψ_D and Π as a function of molecular area A, phases of the monolayer can be correlated with changes in the surface potential. For DPPC, Ψ_D has a rather exotic behavior which not obeys a simple reduction of the molecular area A, $\Psi_D \propto 1/A$. It is instead obvious to state that each phase of the monolayer the lipids provides a particular contribution to the dipole potential. At room temperature Ψ_D is fluctuating around zero in the (G) phase but at the collapses of this phase at the formation of the continuous (LE) phase, a dramatic increase in Ψ_D from 0 to 310mV is observed but in the pure (LE) phase the potential raises constantly to about 350mV. From the middle of the coexistence (LE-LC) region the constant increase is replaced by steeper ending at 500mV at the transition to the (LC) phase *[Discher2002] [Vogel1988]*.

One should expect that a subphase containing sodium chloride reduces the dipole potential due to a shielding of the phosphate and amino group of DPPC. This is reported (*fig. 4.4*) not to be the case. Instead, an ionic strength of 100mM NaCl only shifts the dramatic increase of the dipole potential at the formation of the (LE) phase toward a higher molecular area *[Nakahara2005]*.

The width of the (LE) phase and the (LE-LC) region is known to depend on the temperature of the monolayer. With a subphase of 150mM NaCl, it is shown in *fig. 4.5* by *[Shapovalov1998]*, that only at temperatures near the critical ($T_c = 40^oC$) a decrease of the dipole potential is observed. The dramatic increase at the beginning of the (LE) phase remains but is broadened. The absence of the (LE-LC) region and the constant increase in Ψ_D until the monolayer collapses, then reflects a characteristic behavior of the dipole potential in the (LE) phase.

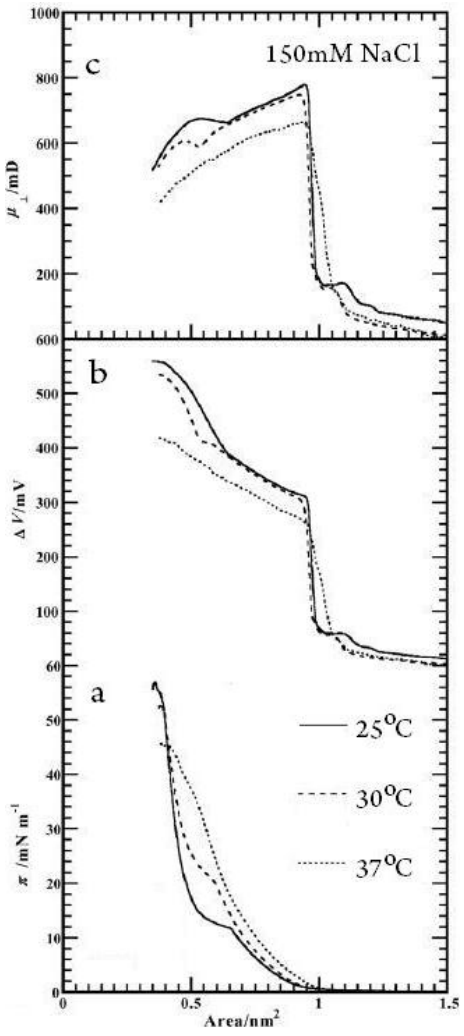

Fig. 4.5: DPPC isotherm (a) and dipole potential (b) at different temperatures with a 150mM NaCl subphase. (c) Dipole moment normal to the monolayer $\mu\perp$ calculated using eq. (4.1). Adapted from [Nakahara2005]

It is then obvious to ascribe the enhanced increase of
the dipole potential in the coexistence region at room temperature, to the total area of domains and conclude that domains have a higher dipole density that the (LE) phase.

4.3 Other Approaches

The discussion between scientist regarding the interpretation of $p_\perp$ from dipole potential measurements on monolayers is ongoing. It will not be preceded here but the ideas are mentioned. The main concerns are the contributions terminal methyl groups of the hydrocarbon chains, the polar head groups and their interplay with water. Common for the models of DPPC is the line of arguments which begins with an underestimate of the polar choline groups since the positive amino groups stick deep into water of high permittivity. Followed by this is an emphasized contribution of the terminal methyl groups on the carbon chains, first suggested by *[Davies1955]*. This has been approached by a three-layer model *[Demchak1974]* by assigning a relative permittivity ϵ_n and a dipole contribution $p_{\perp n}$ to each layer. The subscript denotes the 1. subphase, 2. head groups, 3. Hydrophobic carbon chains. The three contributions are added (due to additivity of dipoles) such that a total dipole potential is calculated with an extended Helmholtz equation:

$$\Psi_D = \frac{1}{A\epsilon_0}\left[\frac{p_{\perp 1}}{\epsilon_1} + \frac{p_{\perp 2}}{\epsilon_2} + \frac{p_{\perp 3}}{\epsilon_3}\right] \tag{4.3}$$

With this model *[Taylor2000]* calculated, for DPPC, the dipole moments for a methyl group and a head group to be 0.236Debye and 0.316Debye. A simplified two-layer model by *[Vogel1988]* in which the headgroups and the subphase contributions are lumped together in one term, isolates the methyl term for further calculations. By this model the contribution from the terminal methyl groups of DPPC was calculated to be 6/7 of the dipole moment and 1/7 was ascribed to the head groups and subphase. This is widely discussed in *[Brockman1994] [Taylor2000] [Clarke2001]*.

Interpretation of the Brownian motions of domains caused by the mutual repulsion in DMPC monolayers, *[McConnell1990] [McConnell1993]* estimate a differences of the normal dipole components of domains and the surrounding liquid phase to be 260mV.

By investigating the orientation of a fluorescent probe embedded in a DPPC monolayer, three different orientations of the headgroup are identified. Each corresponding to the three regions (LE-LC)-(LC)-(S) with the changes at the phase transitions *[Teissie1994]*. Then a combination of these results with the area covered by domains, let them to propurse that domains in the (LE-LC) region have cores of lipids in the solid (S) phase and a circumference o lipids in the (LC) phase.

B

NOTICE:

Without having discussed the layer-models in detail it can be stated that underestimations of the intrinsic large dipole moments of the headgroup and the ordering of water, leads to overestimation of the terminal methyl groups. The rough calculation of the intrinsic dipole

moment of the choline group ($\approx$ 20.2Debye) yields a dipole potential of 200mV which is below the reported 500mV for a DPPC monolayer. It is plausible that detailed knowledge of charge distribution in the head group and structured water including permittivity of water would result in dipole potentials closer to the measured values.

Sodium chloride will be used to increase the conductivity of the subphase in the experimental work with electric fields. Relative to a pure subphase, the $\Pi - A$ isotherm is more or less unchanged by using a subphase of 100mM NaCl. The increase of the dipole potential at the formation of the (LE) phase is shifted toward the gaseous phase with $\approx 10\mathring{A}^2$/molecule *[Shapovalov1998]*. This concentration of sodium chloride, however has no influence on the coexistence region or the dipole potential and the dipole moment of the lipid domains.

It can be stated that domains in the coexistence region has a higher dipole moment than the surrounding liquid phase.

.l-

Chapter 5

Materials and Methods Combination of Fluorescence Microscopy and Applied Electric Field

Description and considerations of the used combined setup are given; Langmuir trough, fluorescence technique, optics, electrical stimulation and setup.

5.1 Langmuir Trough for Isothermal Compression

The same Langmuir trough used for both normal isothermal compression and electric field experiments is shortly described in this section focusing on the experimental conditions for isothermal compression. The results of isothermal compression of DPPC monolayers are presented in Chapter 3

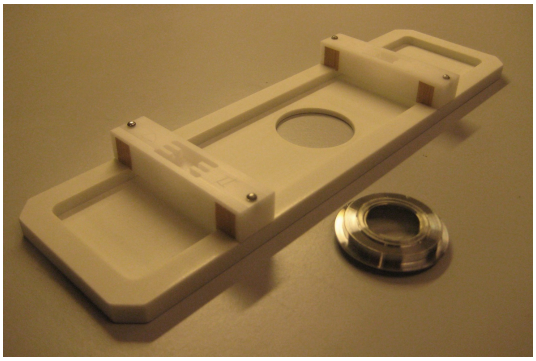

Fig. 5.1: Langmuir trough used for both normal isothermal compression of DPPC monolayers and for experiments with an applied electric gradient field. The trough is described in the text above.

The Langmuir trough used was made of teflon containing 20% glassfiber with inner dimensions of 20cm x 5cm x 0.5cm, *fig. 5.1.* The glassfiber made the trough less flexible and the two barriers used for compression were made of Delrin which is less hydrophobic than glass-teflon. Their two contact angles of the water are respectively 45^o and 90^o

[Hardy2006]. The barriers slide easily on the cliff of the trough and sticks 1mm into the subphase. Four peaces of teflon coated tape are placed on both sides near the end of the barriers and in contact with the trough and the subphase. This avoids leakages of lipids into the tiny space between barriers and trough and under the barriers. To allow optical focusing on the water-monolayer interface the trough was equiped with a cover glass mounted on a ring of stainles steel inserted into the bottom of the trough. A claning procedure and a method for gluing the coverglass onto the steel ring are provided in Appendix A.3 and A.4.

Materials used in this work

Symbol	**Description**	**Data**
Camera EMCCD	Electron Multiplying Change Coupled Device	chip array 512 x 512
Delrin	Polyacetal Engineering Polymers, Trough barriers	
DPPC(1.)	1,2-dipalmitoyl-sn-glycero-3-phosphocholine	734.05g/mole
Ethanol	ethanol lipid solvent	99.9% (pure)
Hexane	n-hexane lipid-ethanol solvent	
Teflon	Poly(tetrafluoroethene), Trough	
TRITC-DHPE(2.)	n-(6-tetramethylrhodaminethiocarbamoyl)-1,2-dihexadecanoyl-sn-glycero-3-phosphoethanolamine, triethylammonium salt	1236.67g/mole
Wire of $_{40}$Zr(3.)	Zirconium. diameter 0.127mm	$\rho = 421\text{n}\Omega\text{m}$
Plate of $_{78}$Pt	Platinum plate 0.2mm x 5mm x 10mm	$\rho = 105\text{n}\Omega\text{m}$
Power supply DC	for electric field	0 - 2500V
Power Switch(4.)	fast push-pull of the electric potential 0-3000V	$\tau = 10^{-9}$sec.

(1.) Avanti Polar Lipids, Al. USA

(2.) Invitrogen, Cal. USA

(3.) FOOTE Mineral Co., Phila. USA

(4.) Behlke, Kronberg, Germany

Materials and Method for Monolayers
The lipid monolyers were made from DPPC (1,2-dipalmitoyl-sn-glycero-3-phosphocholine) dissolved in n-Hexane/Ethanol (95/5 vol.%) at a concentration of 0.5mg/ml or sometimes 0.7mg/ml with the relative amount of the fluorophore (TRITC-DHPE 0.1 to o.2 mol%). The lipid-fluorophore solution was spread from a pipette in droplets of 0.5μl to 0.7μl on the subphsase containing 150mM NaCl originately disolved in pure milli-Q water, 18.2 MΩ restitivity. All experiments were carried out at room temperature, $20 - 24^oC$. A heat-bath was used in the individual experiments to stabilize the temprerature in combination with a thermocouple mounted at the trough bench inside the cover box. Compression rate were usually $0.8\mathring{A}^2$/molecule/min. or $1.5\mathring{A}^2$/molecule/min. Experimental conditions will shortly be mentioned while the results are pressented.

1mg TRITC-DPHE was dissolved in 4ml ethanol (99.9%) in its plastic tube and removed to a clean tube over 4 trials of each 1ml ethanol to have a final density of 0.25mg/ml i.e. a concentration of 0.2mM.

5.2 Fluorescence and Optics

This powerful technique applied to monolayers can be used to study morphology, single particle tracking, diffusion and a warty of catalyzed surface processes. The development of the technique took the beginning in 1981 with the first combined Langmuir trough and epi-fluorescence microscope and uncovered the mysterious behavior of phospholipid films at air-water interface, *[VonTscharner1981]*. The revolution in the field came with the construction of the first inverted fluorescence microscope 3 years later and serious monolayer studies now relie on this idea [Loesche1984]. With the wide field fluorescence microscopy (WFM) setup used in this work, high resolution images of the morphology of DPPC monolayers can be obtained and the important feature , additional instruments can be applied from above.

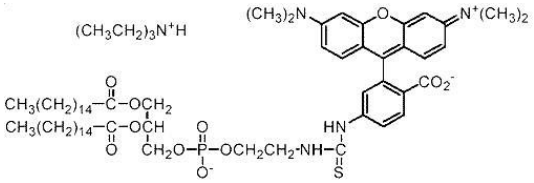

Fig. 5.2: TRITC-DHPE fluorescent molecule soluble in liquid (LE) phase and has low solubility in water. Wavelength of max. excitation λ_{ex} = 540nm = $9.7{\cdot}10^{-19}J$ and emission λ_{em} = 580nm = $9.1{\cdot}10^{-19}J$. [www.invitrogen.com].

TRITC the Fluorophore used
The fluorophore used in this work is TRITC which is a derivative of the often used Rhodamine. The fluorophore is contained in the TRITC molecule which is attached to the ethanolamoine headgroup of the phospholipid DHPE, *fig. 5.2*. DHPE has 2 hydrocarbon chains of each 16 C atom, just as DPPC. It was chosen due to its ability to fit into the lipid matrix of DPPC molecules forming the monolayer. The relatively large TRITC molecule does not complicate the lipid matrix if it is used in small amounts, normally 0.1 - 0.2mol% and has low a solubility in water, mostly because of the hydrophoic hydrocarbon

chains. It is only soluble in the liquid expandedn phase of the monolayer, but not in the gel and gaseous phases. This means that its fluorescence function is normal in the liquid phase.

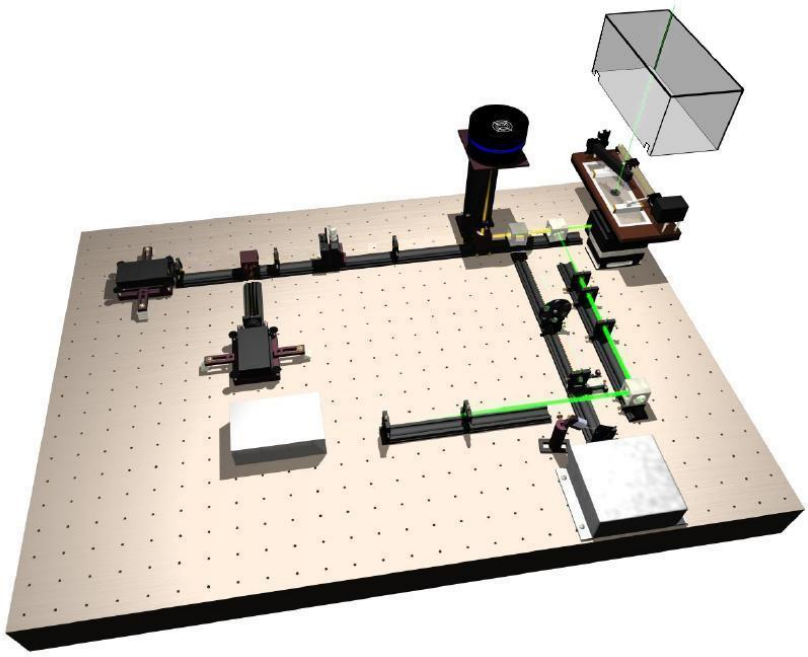

Fig. 5.3: Overview of the beam line of the wide field fluorescence microscope and the Langmuir trough mounted in the trough bench. Components are used as described in the text. Torus laser, beam expander, Lenses (L1) (L2) (L3), Dichroic mirror, Langmuir trough, Acrylic cover box, Flip mirror, EMCCD camera. The information path for this combined setup is sketched in fig. 5.6.

Fluorescence and Related Problems

I general fluorescence occur when a molecule relaxes to its ground state S_0 emitting a photon after being excited to its first electronically excitation singlet state S_1. The excitation happens if the fluorophore absorbs an incoming photon with the required energy i.e. wavelength. Equation 5.1 relates the energy and wavelength of a photon.

$$E = \frac{h \cdot c}{\lambda} \tag{5.1}$$

h is the Planck constant $6.6 \cdot 10^{-34}$Js and c the speed of light in vacuum $3 \cdot 10^{8}$m/s. Due to the molecular structure of TRITC the energy levels S_0 and S_1 are close in the sense of energy. The emission energy E_{em} is somewhat lower than the excitation energy E_{ab} because of internal vibrations in the fluorophore, thus the wavelength of the emitted light is longer than the absorbed light. For TRITC $\lambda_{ex} = 540\text{nm} = 9.7{\cdot}10^{-19}$J and $\lambda_{em} = 580\text{nm} = 9.1{\cdot}10^{-19}$J. The excitation and the emitted light beams of different wavelengths can be separated by a dichroic mirror such that the emitted light can be analyzed. This is the corner stone in fluorescence microscopy.

There are also alternative unwanted pathways for this conservation of energy like non-radiative relaxation and phosphorescence. They could not be observed to have influence on the monolayer results so they are briefly mentioned next. Non-radiative relaxation take place if the excitation energy is transfered into vibrational energy and dissipated as heat if the molecule interact with another molecule. The latter is called quenching. These pathways and some additional are summarized in a Jablonski diagram with the characteristic time scales of the effects *fig. 5.4*. However all these effects can be included in

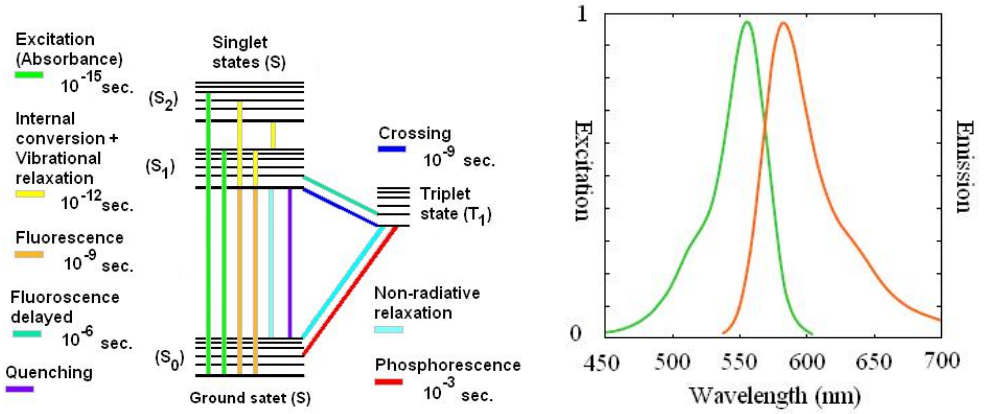

Fig. 5.4: Jablonski diagram of fluorescence showing possible conversion paths.

an "efficiency" of the fluorophore called the quantum yield, Φ which can be experimentaly determined as a relative of the number of emitted photons to photons absorbed in a time interval

$$\Phi = \frac{k_f}{k_f + \sum_n k_n} = \frac{no.\ of\ photons\ emitted}{no.\ of\ photons\ absorbed} \tag{5.2}$$

where k_f and k_m are rate constants for respectively the emission and other effects with no fluorescence. TRITC appears to have a high quantum yield and could be used in smaller amounts than other fluorophore.

More important in this work is the total deactivation of the fluorophore called bleaching. Bleaching can occur if the fluophore reacts with oxygen e.g. when it is exposed to air it will then be a matter of time before this reaction causes the fluorescence cycle to stop. In a monolayer study like this work, that kind of bleaching can be neglected. Instead it turned out that use of high laser intensity was the major cause of bleaching so obtaining nice imaging of the monolayer was always a compromise.

Laser - Optics and Imaging

The used WFM was optimized for single particle tracing before this work. This means that the setup was over tuned for this work and the critical laser power required for single particle studies and all the fine adjustable parameters could more or less be neglected. This is a fast travel through the optic table sketch in *fig. 5.3* including technical information and basic theory when needed.

It was assumed that an applied electric gradient field would have changed the shapes and edges of the lipid domains. Imaging of such changes required high optical resolution produced from an immersion media objective of high magnification. Such objectives have high Numerical Apertures (NA > 1) and very short working distances (WD) typically of 100μm - 200μm. NA is a unit less number that defines the size of the focus point i.e. the optical resolution. More strictly

$$NA = n \cdot \sin(\theta_{cone}) \tag{5.3}$$

where n is the refractive index of the immersion media 1.00 for air 1.2 for pure water and θ_{cone} is the half of the maximum angle of the light cone entering the objective. The working distance is defined as the shortest distance from the focus point to the objective which is the outer glass covering the lenses see *fig. 5.5*. Thus, (WD) is includes the thickness of the coverglass 170μm and the level of the water above this glass. Further more the distance from the water to the electrode was at least 200μm. For practical reasons high (WD) was used which enabled using of the focus point to locate the top electrode above the water. The field only caused small changes of the water level < 2μm estimated without lipids. This effect was neglected.

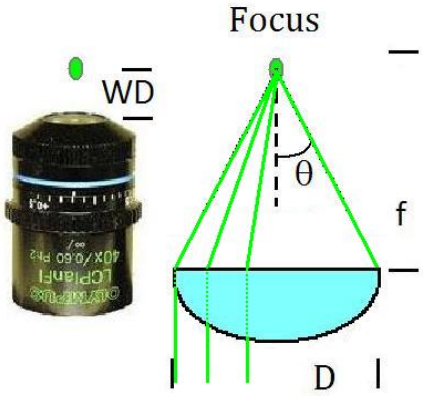

Fig. 5.5: Infinity corrected objective used in monolayer experiments and introducing definitions. No immersion media, 40x magnification, WD = 2.15mm, NA = 0.6, f = 4.5mm

Constrained by the required (WD) and a high optical resolution the choice felt on LCPlanFl 40x see *fig. 5.5* which fitted the conditions very good. Data of objective: Olympus LCPlanFl 40x, NA = 0.60, WD = 2.15mm, Flat field correction i.e. the normally projected curved image is corrected to a flat image. Fluorite correction for green and blue light. Correction to infinity image distance and for a 0.17mm thick cover glass.

Excitation of the fluororphore happens at a wavelength of 532nm *green light* using a 200mW torus laser (Laser Quantum, GB) with a beam wide of $\omega = 0.85$mm. To ensure full limitation of the back focal plane of the objective the narrow gausian beam from the laser was expanded by two lenses (L1) and (L2) with the focal lengths of respectively 12.5mm and 200mm. The expanded laser beam then had a width of

$$\omega_{expand} = 0.85mm \frac{200mm}{12.5mm} = 14mm \tag{5.4}$$

This is much higher than the diameter of aperture of the chosen objective 5.5mm. Not to loose beam intensity by over illumination of the back focal plane of the objective the beam was truncated by a lens before entering the objective (L3). This has focal length of 300mm and was positioned to ensure full illumination of the back focal plane of the objective. The laser beam was directed through a dichroic mirror and reflected vertical up

into the objective by a 45^o mirror (not shown in figures). Emitted *yellow* light from the excited fluorophore in focus enter the objective and travel back the beam ray path but is separated from the *green* laser beam by a dichroic mirror. Finally a camera lens focuses the fluorophore light into a EMCCD camera for analyzing. The beam paths and detection are schematized in *fig. 5.6* for an easy view.

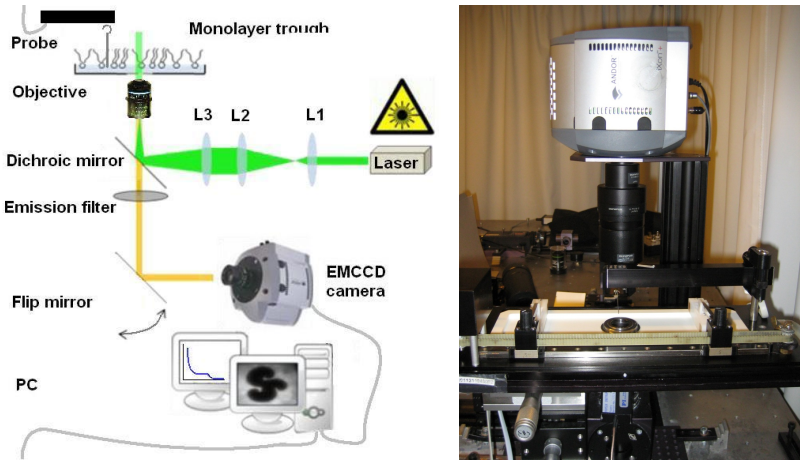

Fig. 5.6: The combined setup of fluorescence microscopy and Langmuir trough used for isothermal compression of DPPC monolayers and real time imaging of the monolayer. The lenses (L1) and (L2) serve as a beam expander. (L3) focus the laser beam to a broad beam entering the objective thus back focal plane of the objective is widely illuminated.

Emitted light from the fluorophore was imaged with a special CCD camera with in-built electron multiplying gain enabling use of lowered laser intensity for excitation of the fluorophore. Bleaching of the fluorophore was still a problem for longer time recordings. However, the resolution of the final image is determined by both the resolution of the microscope objective and the CCD chips in the camera. The optical resolution R of the objective is defined by the Rayleigh resolution criterion *[Rayleigh1879]* which states that two point sores of equal intensity can just be resolved with by the first minimums of the diffraction circles from the two sources. Graphically explained in *fig. 5.7*. Given by the wavelength of the entered light into and the total NA of the objective

$$R = 0.61\frac{\lambda}{NA} = 0.61\frac{580nm}{0.6} = 0.59\mu m \tag{5.5}$$

The second part in optimized imaging is determined by digital CCD camera resolution i.e. the number of pixels available and the dimensions of those. The EMCCD has a pixel array of 512×512 pixels, each of size 16μm $\times$ 16μm. With the chosen microscope objective of magnification 40x and camera lens 1x, the Rayleigh resolution is then magnified and and recorded on the chip array as 0.59μm$\cdot 40 = 23.6\mu$m. This is 1.5 larger than one chip size which is somewhat in the lower limit of the recommended factor 2 for optimal imaging. Originally, the factor of 2 is derived for optimized distinguishing between two signals in telegraphy. A signal with frequency width B requires a frequency bandwidth of $2B$ Nyquist

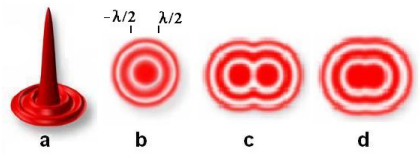

Fig. 5.7: Intensity profile of emitted light from a point source **a** *and its projected Airy disks* **b**. *Optic Rayleigh resolution R is defined in* **c** *as the shortest distance of separation of two intensity centers exactly when the first two intensity minima overlaps. Distinguishing of the sources in* **d** *requires gaussian fitting.*

1928 *[Nyquist2002]*. No matter the theory of signal transmission, the obtained images of the monolayers had an accuracy slightly bellow 1μm illustrated in Sec. 3

5.3 Langmuir Trough and Applied Electrical Gradient Field

This section describes the experimental conditions for generating the electric gradient field used to manipulate the monolayer. The results of these experiments are presented in chapter 6.

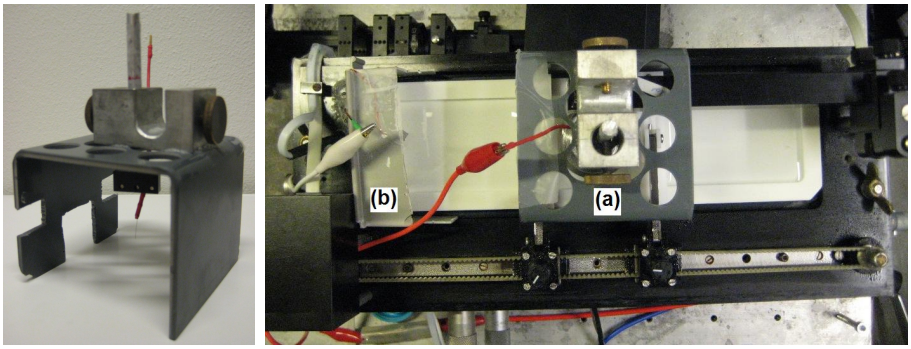

*Fig. 5.8: Self made holders for top (***a***) and sub (***b***) electrodes between which the electric field is generated by an applied voltage.* ***Left:*** *The top electrode had to be adjustable in height and also allow free movement of the barriers. The holder was mounted into the space between the trough and the trough bench, and can be moved along the trough.* ***Right:*** *Top view without the cover box. Sub and top electrodes are connected to a power supply and a switch. The electric connections and conveying of data is illustrated in fig. 5.9.*

It was of highest importance to keep the monolayer non-contaminated during experiments mainly from airborne dust and particles. The decided long equilibration time for the experiments with induced domain free or induced domain cluster required and enclosing of the system. For this purpose two provisional electrode holders were build to fit into the gap between the trough and the trough bench and were kept low enough to use the acrylic cover box see fig 5.8.

Another important criteria of success was the accuracy of the distance d_0 between the monolayer and the top electrode since the strength of the electric field is related to d_0 as

$\propto 1/d_0$. This distance was measured with lens (L3) removed and and observation of the reflected laser light when focused on the electrode tip. The accuracy of d_0 was estimated to 10μm i.e. 5% deviation for the lowest distance used. This method for locating of the top electrode is described in Appendix A.5.

The electric field is generated between the 127μm thick and 1cm long top electrode held a distance of d_0 above the monolayer, and an electrode submersed into the subphase far away behind a trough barrier. The thickness of the top electrode gave a constraint on how close it could be positioned to the monolayer if a suck up of monolayer on the electrode should be avoided. This is caused by the high surface tension of the monolayer-water. When applying an electric gradient field, the polar water molecules align parallel to the field which then exerts a force on the water molecules in direction of the center of the field. This results in an increase of the water level. The connecting wires from the power supply to the electrodes had a normal low resistance of 0.2Ω. Both top and subphase electrodes were chosen to have high electrical conductivity and were made of respectively Zirconium and Platinum. The latter also had the capability of negligible reduced conductivity caused electrochemical reaction with the subphahe. This reaction eq. (5.6) involves hydrogen and forms hydroxide if a negative potential is applied.

$$H_2(g) \rightleftharpoons H^+(aq) + e^- \tag{5.6}$$

Replacing the Platinum with a silver electrode would have caused a difference in its conductivity depending on the polarity of the voltage applied between the top and subphase electrode. A silver electrode will produce silver chloride on its surface if the polarity applied is positive. A negative polarity reject the chloride into the subphase and neutralize the silver, forcing the reaction eq. (5.7) to the right *[Skoog1982]*.

$$AgCl(s) + e^- \rightleftharpoons Ag(s) + Cl^-(aq) \tag{5.7}$$

The high voltages needed for manipulation of the monolayers in this work initially turned out to complicate things and several precautions were taken. Previous published experiments and pilots highly emphasized a controlled strength of the applied field spanning 10^5V/m to 10^7V/m. The field was generated by a high voltage power supply (0 - 2500V) connected to a very fast push/pull switch controlled with a gaiting voltage difference of 5V from a computer connected power supply (ID Instruments). Without such switch and only the high voltage power supply a build up of charges on the top electrode would be much slower and initially effects in the monolayer could not be distinguished from slower effects. The electrical connection of the components used is sketched in *fig. 5.9*

The switch (Behlke, Germany) is very impressive and highly suitable for controlling high a voltage. It is actually a MOSFET switch that requires a maintained supply of maximal 5V to be active. Both charging of high voltage difference (push) and discharging of the circuit when switching it off (pull) is exceptionally fast. The push/pull times are in the order of 10^{-9}s. Two resistors of each 1kΩ were put in between the MOSFET's and

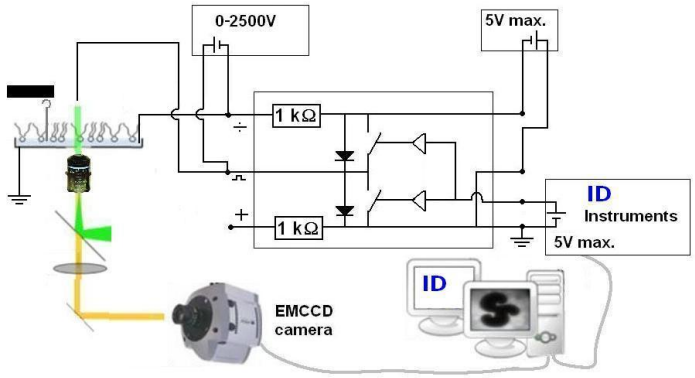

Fig. 5.9: Sketch of the computer controlled electric gradient field and data path of fluorescence microscopy. The field was generated by a high voltage power supply (0 -2500V) connected to a very fast push/pull MOSFET switch controlled with a gaiting voltage difference of 5V from a computer connected power supply (ID Instruments). The MOSFET switch requires a maintained supply of 5V for being active.

output. This functioned as a fuse if a short circuit in case of the mentioned problem with an accidental connection between the subphase-monolayer and top electrode.

Chapter 6

Induced Changes of Monolayers by Electric Gradient Field

After an introduction to the subject the experimental considerations and progress are described. These were used to design the final experiments and setup. The final results are then presented and in the last section a model based on electrodynamics is discussed.

6.1 Introduction

The original question of inspiration for the experimental work in this thesis was *"How does electrical stimulation of a nerve affect the main membrane components - the lipids?"* The question was approached by studying the effect of an electric gradient field applied to a model membrane resembled with an artificial lipid monolayer in a Langmuir trough. The monolayer was made of the lipid species with the highest mass percentage representation in non-myelinated nerves. These lipids are the Diacyl-PhosphatidylCholines (PC's) with their characteristic polar choline head groups *[Sackmann1995]*. To have the model system as simple as possible one species was chosen namely DPPC *fig. 6.1*. At room temperature DPPC monolayers can be compressed into any state and have a broad coexistence region (LE-LC) containing a liquid and a condensed phase. This region is of interest since biological membranes have very broad melting transition profiles and thereby a broad region of coexistence containing phases of the different lipids present in the membranes *[Heimburg2005]*.

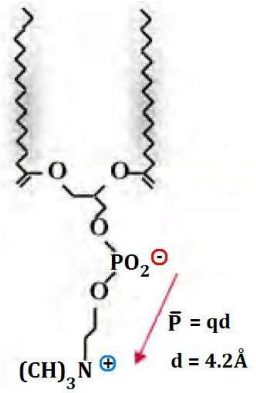

Fig. 6.1: Polar choline head group of DPPC. Given the distance d from x-ray diffraction on multilayers, the dipole moment $\boldsymbol{P} = 6.7 \cdot 10^{-29} Cm = 20.2 Debye$*, 11 times larger than a single water molecule.*

Phase transitions in monolayers induced by mechanical force, temperature, ionic or pH changes are well-studied in the literature as mentioned in chapter 3. Phase transitions controlled with an external electric field are possible if the thermodynamic coupling between the intensive and extensive variable is strong enough, i.e. stronger than couplings in the system that keeps it in a particular state. Temperature and lateral

pressure are clear examples of such intensive variables and phase transitions can widely be demonstrated with the use of isotherms.

An electrical field will then be a candidate for induction of a phase transition in a monolayer of DPPC if the polar choline head groups of DPPC are strongly coupled to the field. The distance between the phosphate and nitrogen is reported in X-ray studies to be 4.2$\mathring{A}$ *[Hauser1981]*. This gives a dipole moment for a single DPPC molecule of the order $6.7 \cdot 10^{-29}$Cm = 20.2Debye[1]. This is an order of magnitude 10 larger than the dipole moment of a single water molecule $\approx 6{\cdot}10^{-30}$Cm = 1.9Debye *[Griffiths1999]*. However the dipole moment decreases when the head group is submersed in aqueous media because of interaction with neighbor lipids and ions in the subphase. Water molecules in the subphase are thought to order around the polar head groups, forming layers of water giving a small increase in the density of dipoles. The dipole potential increases dramatically during compression of the monolayer into the (LE) phase from zero in the (G-LE) region and reach a maximum $\approx$ 600mV in the solid (S) phase *[Nakahara2005] [Vogel1988] [Shapovalov1998]*. This indicates a larger surface normal component of the dipole moments for the condensed lipid domains than the more disordered liquid (LE) phase. Earlier studies described in chapter 1.4 claims that this difference is responsible for movements of lipid domains if an electric gradient field is applied to the monolayer *[Florsheimer1989] [Florsheimer1990]*. The setup for the electric gradient field used was strongly inspired by the original setup of Möhwald and co. workers *fig. 1.4* but instead of $10\mu m$ a $127\mu m$ thick top electrode is used in this work.

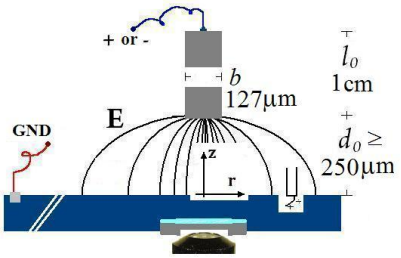

Fig. 6.2: Schematic of the electric gradient field $\boldsymbol{E}$ *with the grounded subphase electrode behind a barrier and the top electrode of length* l_0 *held a distance* d_0 *above the monolayer. The monolayer plane is defined at* $z = 0$ *and the center of the field is defined at* $r = 0$.

The original question has been reduced to how an electric gradient field influences a Langmuir monolayer of DPPC. The gradient field is produced by a voltage difference between an electrode hanging above the monolayer and a grounded conducting subphase. This setup and electric field are illustrated in *fig. 6.2* and defines the coordinate system, the distance d_0 between the monolayer and top electrode, the length of the electrode l_0 and diameter of the electrode b.

Without knowing the distribution of the field in detail it can be stated that it is non-homogeneous and is, in essence, a gradient field. Furthermore, the field is independent of rotation around the z-axis; thus the force exerted by the field on the dipoles in the monolayer is radial from the center of the field, $r = 0$. The direction of the radial force depends on the polarity of the potential applied between the electrodes. Since the dipoles are oriented into the subphase, a positive potential is applied to the top electrode (building up a positive charge) attracted the dipoles and will move them toward the center. This increases the density of lipid domains in that region around $r = 0$. For a negative potential the dipoles are repelled radial from $r = 0$, decreasing the density of lipid domains. The

[1] 1Debye = $3.335{\cdot}10^{-30}$Cm

direction of the force is best illustrated in *fig. 6.3* with a dipole between two angled capacitor plates producing a gradient field because of changing distance between the plates.

A secondary effect of the field is a torque on the dipoles. This tends to align them in the direction of the field lines thereby minimizing the energy of the dipole. This aligning would increase the normal dipole component and hence the force on the dipoles. Because of the structural orientation of the polar choline groups, parallel aligning might favor an increase of the force in the case of attraction of the domains but a decrease it in the case of repulsion. The basic themes for this chapter are now introduced. Important parts of the experimental development/progress and experimental limitations are described below. These considerations leaded to the final method condensed in Sec. 6.3 and was used to achieve the main results presented in Sec. 6.4. Experimental results are theoretically discussed parallel with electrodynamics models of the system in Sec. 6.5.

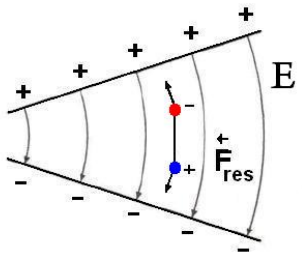

*Fig. 6.3: The force **F** from a electric gradient field **E** on a dipole pointing in the same direction of the field.*

6.2 Preliminary Results and the Experimental Progress

All the monolayers in the experiments presented in this chapter was spread with the standard DPPC solution on a 150mM NaCl subphase described in Section 5. The monolayers were compressed to a lateral pressure of 30mN/m and then fully expanded in order to check the setup and ensure equal conditions for the monolayers. A representative compression isotherm is shown in *fig. 6.4* for a monolayer at 22.7^oC. Before the electric gradient field was applied, the monolayer was compressed into the coexistence region to the lateral pressure of interest.

Two of the first experiments with applied field

These two experiments **a** and **b** recovered the effect of the electric gradient field *fig. 6.2* were carried out with a primitive setup of the electrodes. These two results gave further experiences which were used to construct the final setup. Attraction of lipid domains in the monolayer with a positive electric potential applied to the top electrode is first demonstrated in experiment **a**. Repulsion for the opposite sign for the potential is not shown. The troublesome influence of drift in the monolayer is observed in experiment **b**.

The top electrode was held between 500 and 600μm above the monolayer and the water level was at 500μm above the coverglass in the trough. This was tried to be held constant by compensating for evaporation. The camera lens had 1x magnification and a 40x air objective in the first and 20x in the second experiment were used.

Spatial location of the top electrode was at this early stage simply found by turning down the sensitivity of the camera and illuminate above the electrode. It was then possible

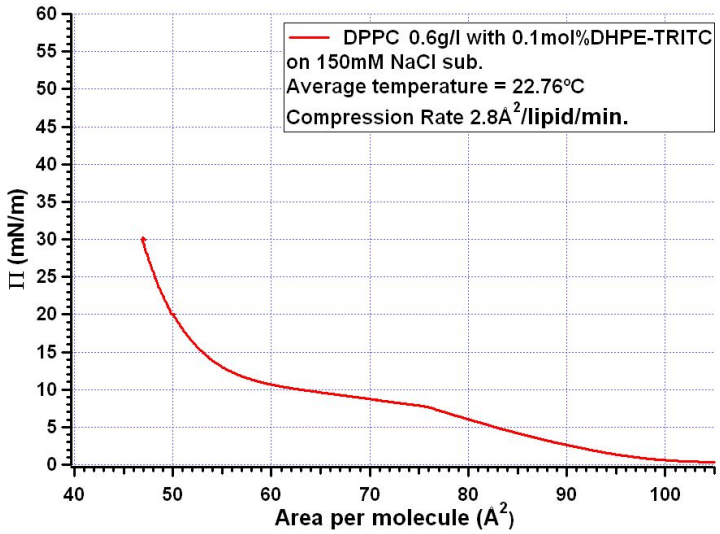

Fig. 6.4: Representative isotherm of DPPC monolayer at 22.7°C for the combined experiments of isothermal compression and applied electric gradient field. The amount of TRITC-DHPE used in the monolayers in these experiments varied from 0.1 to 0.2 mol%. Such small amounts could not be observed to influence the isotherm or the domains in the coexistence region.

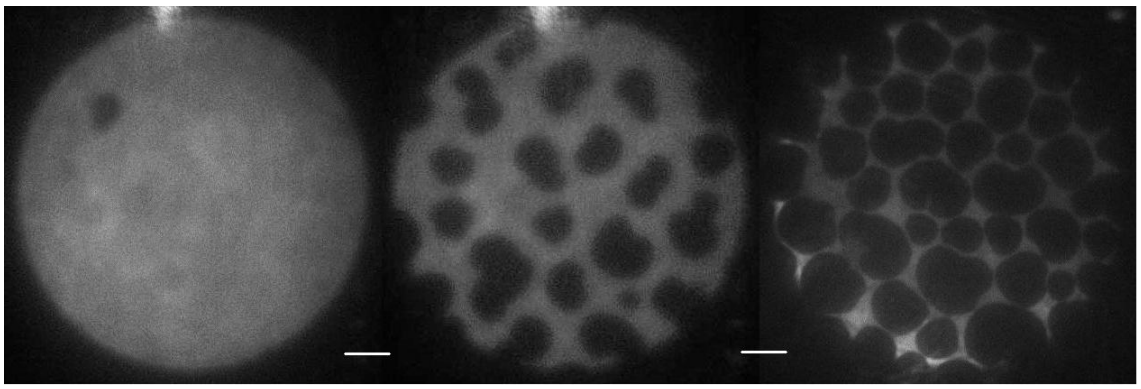

Fig. 6.5: ***Experiment a.*** *At a Lateral pressure of 10mN/m domains are observed.* ***Left:*** *Before the electrical field was applied domains was observed in the focus.* ***Middle:*** *After 110 seconds with 500V applied to the top electrode the density of domains was increased due to attraction.* ***Right:*** *After 40min. a packed cluster has formed of mutually repulsive domains.* ***Conditions:*** *Scalebar: 20μm, Mean temperature 23°C, Subphase 150mM NaCl, 0.1mol% TRITC-DHPE, Compression Rate 0.9Å^2/molecule/min., d_0=4000μm.*

to use the microscope and focus on the shadow side and bottom of the top electrode and observe it with the camera. Having found the horizontal and vertical position of the top electrode above the monolayer the focus point was moved down in the monolayer plane. From this the distance d_0 from the bottom of the electrode to the monolayer was given. It was ensured that the illumination was not too strong to damage the camera (photon counts per exposure time $\ll$ 1200). This method for locating the top electrode was not successful every time and the distance d_0 was attached with an accuracy estimated to 25μm.

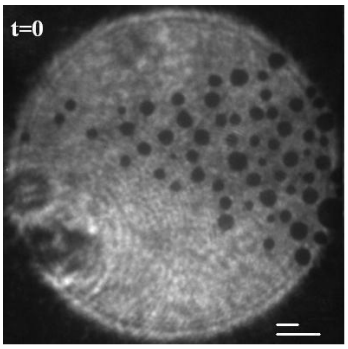

Fig. 6.6: ***Experiment b.*** *The electric potential was reduced from 1000V to 500V on the top electrode just before t=0. A tail of domains was formed because of the drag force from the constant drift in the monolayer. The velocity of the drift is is estimated to* $\approx$ *0.5mm/s.* ***Conditions:*** *Scalebars: Small* $20\mu m$*, large* $40\mu m$*,* $d_0 = 5000\mu m$*, Mean temperature* 21^oC*, Lateral pressure 9mN/m, Subphase 150mM NaCl, 0.1mol% TRITC-DHPE, Compression Rate* $0.9\AA^2$*/molecule/min.*

Experiment a

A negligible drift in the monolayer was observed. By applying a positive electrical potential of 500V to the top electrode it was observed that domains moved toward the center of the electric field located beneath the top electrode ,r=0. The density of domains was slowly but clearly increased in this region *fig. 6.5*. The diameter of the induced domain cluster and domain free area (not shown) exceeds the field of focus by several times.

Experiment b

The conditions was the same in this experiment except that the temperature was kept at 21^oC and the monolayer was compressed to a lateral pressure of 9mN/m before applying the field. Repulsion or attraction of domains was again observed with applied voltages for opposite signs. Significant drift of $\approx$ 0.5mm/s in the monolayer changed the shape of the domain cluster. Because of the drift a voltage of 1000V was applied to grow a domain cluster. A reduction of the voltage to 500V was not enough to keep the diameter of the domain cluster constant with time. After the reduction a tail of domains on the cluster was formed with the drag on the domains is toward the left. The main part of the cluster to the right is not shown in *fig. 6.6*.

Drift and evaporation

The first experiments with the applied electric gradient field were implicated with limiting experimental disadvantages and problems. Determination of the radius was hindered since movement of the focus was constrained by the objective itself and the steel ring in the trough. This was caused by the high water level used for which the space between objective and steel ring was insufficient. The setup for the electrodes was primitive which made it difficult to adjust and localize the top electrode. A plastic bag was used in an attempt to enclose the combined Langmuir trough and electrode setup. The electrode holders

hindered a tight sealing and constant evaporation of the subphase during the experiments was observed. In some of the experiments a large convective motion (drift) in the monolayer was observed. The drift was of the order of 0.5mm/s, so a state of the monolayer close to mechanical equilibration could never be reached during these experiments. Evaporation of the subphase increased the distance between the top electrode and monolayer and thereby decreased the strength of the applied field and its force on the dipoles in the monolayer. In addition, the evaporation of the subphase reduced its buoyancy on the tensiometer probe. In order to avoid drift and evaporation of subphase the primitive method for positioning the electrodes was abandoned.

The improved self-made setup for the electrodes allowing total encapsulation of the monolayer and electrodes is described in section 5.

Constraints and Remarks on the Measurements

It is obvious that attraction of lipid molecules in the monolayer toward the center of the field would increase the density of lipids and thereby increase the lateral pressure. In the coexistence region of interest a small change in lateral pressure corresponds to a large change in molecular area.

It was thought that an induced change in lateral pressure as a function of the applied electric field strength could be measured. To have a large sensitivity in such measurements a change in molecular area could be obtained by adjust the trough barriers to have the pressure constant.

However it was impossible to measure the lateral pressure in that region close to the electrical field. The tensiometer used to measure the lateral pressure was affected itself by the electric gradient field. For the lowest applied voltage of 50V the lateral pressure jumps initially 0.35mN/m then falls back and decays from a value 0.1mN/m above the pressure before the voltage was applied, *fig. 6.7*. The tensiometer has a piezo crystal which transforms the lateral pressure of the monolayer on the probe into a voltage difference for data processing. This effect was also observed without monolayer (only subphase) and also with an empty trough having the tensiometer at the same spatial position.

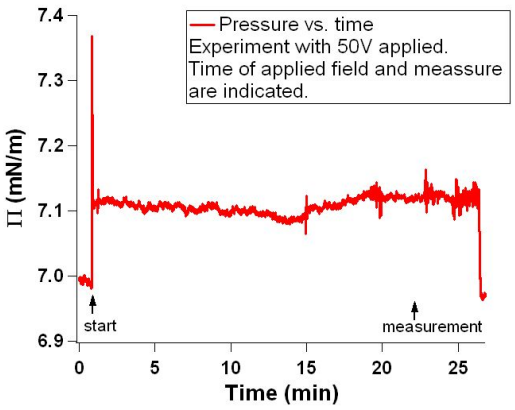

Fig. 6.7: Effect of the electric gradient field on the teniometer with the lowest used voltage $U = 50V$. The tensiometer was held $1cm$ from the top electrode. (start) marks turn on of the field and (measurement) marks the time for measuring the diameter of the induced area in the monolayer.

A self-made probe of glass was tried instead of the normal one of aluminum but without reduction of the effect. It was then chosen to not to pay attention to the lateral pressure and instead keep the area constant during the time when the electric gradient was applied.

It was then tried to experimentally find the time it takes to induce a domain cluster or domain free area and thereby estimate an equilibration radius of the induced area. Unfortunately it appears that these times were very long and the typically area created exceeded

the focus width. The bleaching effect of the fluorophore in focus disabled a prolonged imaging of the induced domain cluster. Bleaching was avoided by having the laser turned off between the appliance of the field and the imaging. This would only give reliable results if evaporation of subphase, contamination and drift of the monolayer could be avoided.

The observed direction of the lipid domain movement was previously reported to have an opposite sign to the direction of predicted by electrodynamics *[Mohwald1986] [Heckl1988]*. The sign of the voltage applied for experiments in this thesis are measured with a voltmeter. The signs of the polarity of the electrical setup used here were finally demonstrated by changing the top electrodes with one made of silver. Both the top electrode and the usual subphase electrode were then immersed into a separated NaCl solution. It is known that an applied positive voltage on a silver electrode creates a layer of silver chloride AgCl which appears black on the silver electrode *[Skoog1982]*. This was the case in this work and the reversed effect was observed for negative applied voltage. The potential driven chemical reaction was discussed in section 5.3.

Conclusion
The two experiments clearly showed that the force on a lipid domain from an electric gradient field was in agreement with the expectations. For a positive potential applied to the top electrode, the field pointed down like the orientation of the dipole moment of the domains. This attracted the domains to the field center, r=0. For opposite polarity of the voltage the field pointed up and the domains were repelled away from the field center. The growth times for induced cluster or domain free area were observed to be of several minutes for weak fields and increased with field strength. These observations of the force and the growth time agrees with previously results discussed in Sec. 1.4, so improvements of the experimental seemed to be fruitful. In spite of the limitations of the initial experiments these effects were defeated and a final setup for the electrodes were developed see Sec. 5. The final setup made it possible to measure the equilibration radius of domain cluster and domain free area as a function of applied voltage.

6.3 Final Experiments and Settings

Experiments were carried out to establish a relation between the applied voltage U and radii of both induced domain cluster and domain free area. Having the monolayer compressed into the region of coexistence the field was applied for 1300s = 22 minutes. This time was used in all experiments because actual equilibration times could not be measured and it was assumed to be longer than the equilibration times. The equilibrium radius R_0 of an induced area was measured with use of the focus field and the micro-screws for horizontal movements of the monolayer trough. With this method the accuracy of the radius measurement was estimated to be $15\mu m$ which included the accuracy of the micro-screws and the fact that the monolayer displaced a little upon moving it due to inertia.

A reliable method for locating the top electrode was developed so the accuracy of the

distance d_0 to the top electrodes is of the order 10μm. With this method the horizontal position of the electrode could be found to be right above the focus point. This was highly needed for the chosen method for collecting the data. A user friendly guide is given in Appendix A.5.

The water level was maintained at 250μm above the cover glass in the trough. This was held constant by moistening the acrylic cover box and compensating for evaporated subphase by adding new from the stock solution (150mM NaCl).

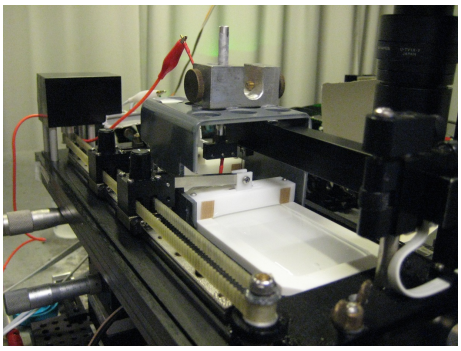

Fig. 6.8: Setup for the electric gradient field applied onto a DPPC monolayer (without the acrylic cover box). See detailed description section 5.

6.4 Results

With the above described improvements manipulation of monolayers with the applied electric gradient field was successful. Creation of a domain cluster is first illustrated. Secondly the radii of induced cluster and domain free areas are measured as functions of the applied voltage.

6.4.1 Creation of a Domain Cluster

With slow isothermal compression of the DPPC monolayer into the coexistence region, the condensed lipid domains that formed were more or less equal in size and homogeneous distributed in the monolayer. A small fraction of oddly developed domains was observed. Distinct behavior of the domains due to their shapes with an applied electric gradient field was recognized but could not be described quantitatively. With the field applied the domains reoriented during the first few seconds. After the reorientation, the movement of the domains was toward the center of the field. For some domains this movement was instant because of an already favorable orientation in the field. *Fig. 6.9* gives an example of these observations during the first 90 seconds with a positive voltage applied on the top electrode was recorded. A domain with an initial favored orientation is marked by an $\multimap$ in the figure. In the first 5 seconds this domain is located 91μm from r=0 and reach a mean velocity estimated to 5.3μm/s during its movement from r=91μm to r=64μm. From this point and to its position after 10 seconds the mean velocity is decreased to 12.8μm/s.

In these experiments with domain clustering, dense packing of domains was observed. For a field with +300V and $d_0 = 150\mu$m the smallest distance between domains was typically of pixel resolution i.e. 1pixel = 0.4μm. But complete contact and fusion of domains leading to condensation into a solid phase was never observed in any of the experiments.

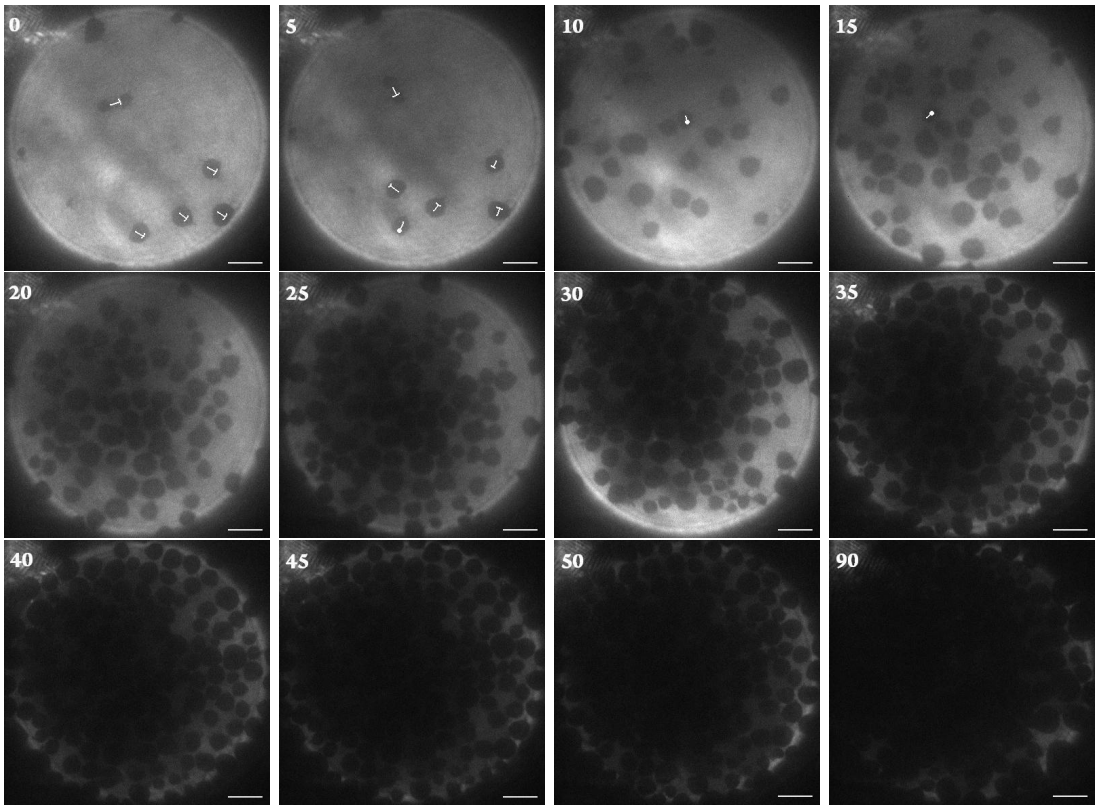

Fig. 6.9: The first 90s of the creation of DPPC domain cluster induced by an electric gradient field applied to the monolayer compressed to a lateral pressure of 7mN/m. Domains are dark shaded while the fluorophore containing liquid phase appears bright. The field was applied at applied at t=0 (top left). Rotation of domains was observed in the first 5s illustrate with the orientation of $\perp$*. After the rotation strong attraction and condensation of domains occurs and morphology of the domains are unchanged during the condensation. Some domains had a favorable initial orientation and are attracted at once,* $-\circ$*. Because of bleaching domain boundaries of domains in the focus field cannot be distinguished.* ***Conditions:*** *Scalebar =* $20\mu m$*, Applied voltage 3000V,* $d_0 = 200\mu m$*, Mean temperature* 21^oC*, Lateral pressure 7mN/m, 150mM NaCl subphase, 0.1mol% TRITC-DHPE, Compression Rate* $0.9\AA^2$*/molecule/min.*

6.4.2 A Voltage-Radius Relation

It was of importance to experimentally find the relation between the voltage U applied to the electrodes and the radius R_0 of the domain cluster and the domain free area. All raw voltage-radius data are plotted in *fig. 6.10* as the radius of the area measured for a given voltage applied in units of μm and V. Zero radius for zero field is assumed as a data point in the plots. There are three data sets of induced domain clusters marked by $\square$ $\bigcirc$ $\triangle$ and two sets of induced domain free areas marked by $+$ $\times$. In general R_0 is not linear with U but the effect decrease for larger values of the voltage applied. The effects of repulsion and attraction of domains cannot be distinguished in the data. Small variation of the temperature has no effect. The relation is mostly pronounced for the data set marked brown $\bigcirc$. The brown data were obtained in the last experiments with the highest degree of experience of the setup. The two values of the lateral pressure 7mN/m and 9mN/m

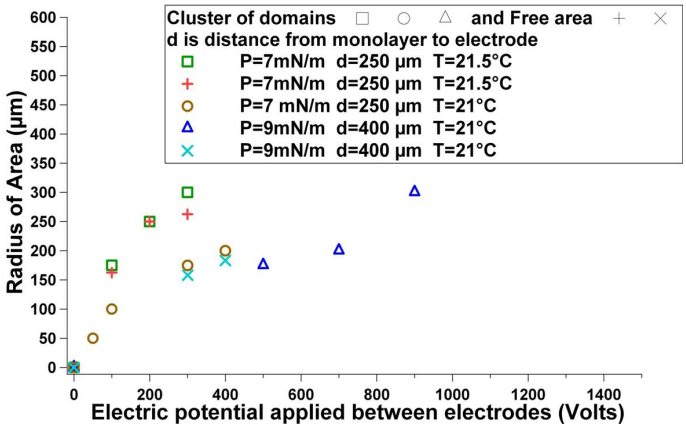

Fig. 6.10: Radius of domain cluster and free area induced by a gradient field of applied voltage U. Accuracy of R_0 is $15\mu m$ and d_0 is $10\mu m$.

measured just before appliance of the field are both in the coexisting region and have no significant influence on R_0. Notice the applied field is weaker for all the data at 9mN/m because of the larger values of d_0. This point is emphasized when the voltage is normalized *fig. 6.11* with the distance d_0 giving the field strength at the center of the gradient field at the air-monolayer interface right below the electrode i.e. r=z=0. The field strength is of the order 10^6V/m.

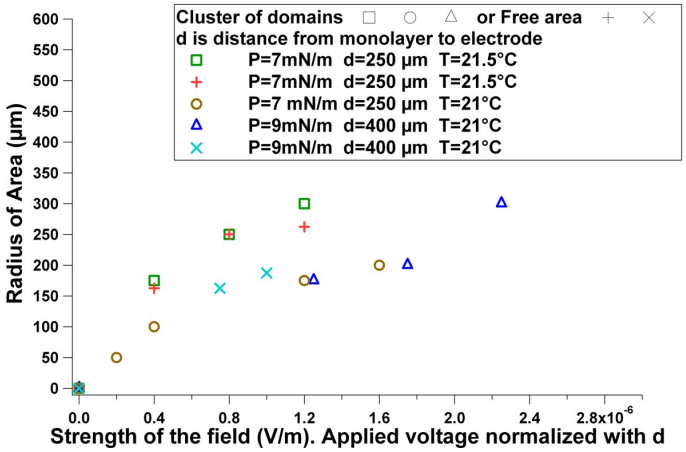

Fig. 6.11: Radius of domain cluster and free area induced by a gradient field of voltage U normalized with the distance d_0 between the monolayer and tp electrode i.e. the strength of the electric field in units of (V/m). Accuracy of R_0 is $15\mu m$ and d_0 is $10\mu m$.

Beside the variation of the data the normalization with d_0 reveals constancy in the data of the effects of the applied electric gradient field. Paying attention to the brown data set they recover the effect of voltage and radius as a power law. This is emphasized in *fig. 6.12* with the radius squared R_0^2 as a function of the voltage U. Within error the data follows straight lines for each series of experiments with similarities among the domain free area

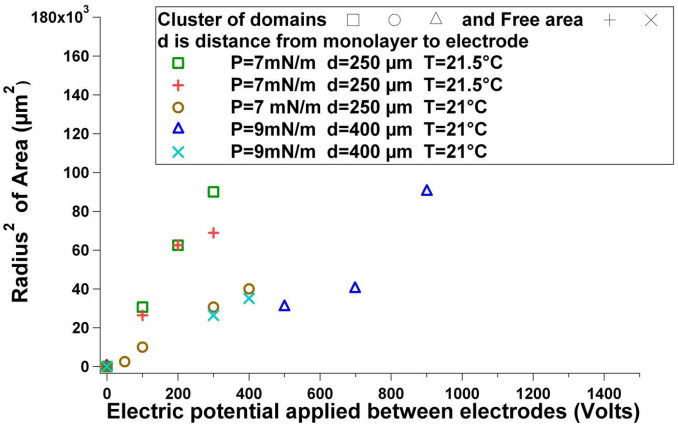

Fig. 6.12: Equilibrium radii of domain clusters and domain free areas squared R_0^2 as a function of the applied voltage U. Note the 10^3 on the y-axis, accuracy of R_0^2 is $225\mu m^2$ and d_0 is $10\mu m$.

and the domain clustering for both values of the lateral pressure. This largely supports the a relation between U and R_0 as a power law R_0^2=K·U. The brown data points exhibits a constant of proportionality K estimated to $100\mu m^2/V$. This agrees with the same order of magnitude with results obtained in *[Heckl1988]*. The dependence on the distance d_0 from the top electrode to the monolayer is hardly recognized from the data. For a small d_0 the field is stronger and one should expect a larger constant of proportionality. Errors of the radii are relative small because the accuracy of the measurement is $15\mu m$.

6.5 Theory and Discussion of the Applied Electric Field and Dipoles

The observed results fully support the idea of the electric gradient fields and dipole interaction. The interaction is best proved by the dependence of the domain movements on the sign of the potential applied. Consequences of this interaction are discussed below.

Force and Dipole Components.
The composition of the head group is known to produce a dipole moment but its direction and thus the direction of the dipole moment of a domain is not obvious. The conformation of the head group embedded in water is not fully understood and even in the presence of an electric field it might change. This was mentioned earlier in chapter 1.4 and chapter 2 where the dipole potential of DPPC monolayers indicate increased density of the dipoles during compression and a reorientation of the dipoles toward the monolayer normal. This suggests a more or less in-frozen dipole moment of each condensed lipid domain pointing down in the subphase and is supported by mutual repulsion between domains.

The exerted force by the field on dipole i is related by $\mathbf{F} = (\mathbf{p}_i \cdot \nabla)\mathbf{E}$. The total dipole moment of a lipid domain $\mathbf{p}$ is a superposition of all dipoles $\mathbf{p} = \sum_i^N \mathbf{p}_i \leq Np$ where N is the number of lipid molecules and $\leq$ because of different orientations of the dipoles. For an

approximately circular domain of radius a the total dipole moment of the domain normal to the monolayer is given as $\mathbf{p} = \pi a^2 \overline{p}$. Followed from the discussion of the origin of the dipole potential in chapter 4 values of the mean dipole density $\overline{p}$ for domains are unclear.

The simple calculation yielded a dipole moment of the choline head group normal to the monolayer in water of permittivity ϵ=80 to be $\overline{p} \approx 0.25\text{Debye}/49\mathring{A}^2 = 5.1{\cdot}10^{-3}\text{Debye}/\mathring{A}^2$.

Deduced from dipole potential measurements on DPPC monolayers $\overline{p} \approx 0.5\text{Debye}/49\mathring{A}^2 = 1 \cdot 10^{-2}\text{Debye}/\mathring{A}^2$.
Since they only differ by a factor of 2 the measured value of $\overline{p} \approx 0.5\text{Debye}/49\mathring{A}^2$ is used for calculations in this chapter which should only be taken an estimate.

Because the field used is independent of rotation around its z-axis (center of the field) a dipole $\mathbf{p}$ in the monolayer plane is given:

$$\mathbf{p} = (p_r, p_z) \qquad \mathbf{E} = (E_r, E_z) \tag{6.1}$$

A third component of the dipole p_ϕ regarding its orientation in the monolayer plane is neglected since the movement of the domains are observed to be radial. The initial reorientation of some domains does not influence the radial movement. The electrical field is derived from the electric potential between the top electrode and subphase:

$$\mathbf{E} = -\nabla\Psi \tag{6.2}$$

This results in the two general expressions for the force $\mathbf{F} = (\mathbf{p}_i \cdot \nabla)\mathbf{E}$:

$$F_r = \left(p_r \frac{\partial E_r}{\partial r} + p_z \frac{\partial E_r}{\partial z}\right) \qquad F_z = \left(p_r \frac{\partial E_z}{\partial r} + p_z \frac{\partial E_z}{\partial z}\right) \tag{6.3}$$

Since the polar head group is embedded in the subphase it is reasonable to put z=0 which leads to simplification of the force components because $\frac{\partial E_r}{\partial r} = 0$ and $\frac{\partial E_z}{\partial z} = 0$. Continuity of the electric potential across z=0 implies that the curl of the field[2] $\nabla \times \mathbf{E} = 0$. Thus the components of the force are:

$$F_r = p_z \frac{\partial E_r}{\partial z} = p_z \frac{\partial E_z}{\partial r} \qquad F_z = p_r \frac{\partial E_z}{\partial r} = p_r \frac{\partial E_r}{\partial z} \tag{6.4}$$

The vertical component of the force F_z is from now neglected since no vertical movement of the domains was observed and the radial component of the dipole moment is $|p_r| < |p_z|$. An electric field of the strength used was not observed to influence the (LE) phase of the monolayer. If the $\mathbf{E}$ field points down into the subphase, a dipole pointing down into the subphase is forced toward the center of the field r=0. If the direction of the $\mathbf{E}$ field is reversed (to upward) the dipole pointing down is force away from the center of the field. This dependence was experimentally observed and is shortly summarized in *fig. 6.13*.

A DPPC bilayer is normally described as a dielectricum with a dielectric constant ϵ=2 with bound charges. If this is also the case for the monolayer, an applied $\mathbf{E}$ field would

[2] $\nabla \times \mathbf{E} = \left(\frac{\partial E_z}{r\partial\phi} - \frac{\partial E_\phi}{\partial z}\right)\mathbf{r} + \left(\frac{\partial E_r}{\partial z} - \frac{\partial E_z}{\partial r}\right)\phi + \frac{1}{r}\left(\frac{\partial (rE_\phi)}{\partial r} - \frac{\partial E_r}{\partial \phi}\right)\mathbf{z} = 0$

induce a charge separation in the dielectricum and attract it into the strongest region of the field. This effect is then independent of the direction of the field. Only the sketched dependence of the field direction was observed in all the experiments, which indicates a non dielectric nature of a DPPC monolayer.

A example of this effect on a dielectricum was found for the clean subphase with an applied homogeneous electric field of an area of 2cm × 20cm across the air-water interface, see Appendix A.1. Thus a field of strength $5{\cdot}10^5$V/m raises the water level about 15μm because of the fringing field (boundary field) of the homogeneous field. However, a rais in the water level with the use of the top electrode for the gradient field was not noticed to rais in any cases.

The Relation between Voltage and Equilibration Radius of the Induced Area

The measured values of R_0 of the clusters of attracted domains and the radius of the domain free areas were found in *fig. 6.12* to be related U as a power law. For a given U the measurements imply no distinction between a cluster and a domain free area.

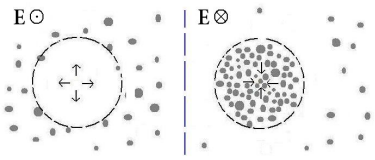

Fig. 6.13: Movements of lipid domains induced with a radial electric gradient field. View from above the monolayer. The direction of the field and the movement of domains are indicated.

Equilibrium occurs because the radial force exerted by the electric gradient field is balanced by a force from the monolayer itself. This balancing force stems from repulsion of domains in the monolayer repelling each other due to dipole-dipole interactions.

An induced circular cluster of domains will then grow in size until, at a distance R_0 where the force from the electric gradient field is equal the repulsive dipole force from the cluster.

For the case of a repulsive gradient force domains outside R_0 are compressed and thereby increase the repulsive forces between the domains outside R_0. Drift in the monolayer can influence the equilibrium and hence R_0.

Torque Excerpted by the Field on the Dipoles.

Furthermore, the applied field exert a torque $\mathbf{N}$ on a dipole tending to align it parallel to the field given as $\mathbf{N} = \mathbf{p} \times \mathbf{E}$. In the case of domain attraction the p_z might increase due to the parallel aligning resulting in a larger radial force and hence a larger radius of equilibrium. For domain repulsion the $\mathbf{E}$ field is antiparallel to p_z which might decrease the force and result in a reduced radius of equilibrium. This is not supported by the obtained results but is reported in *[Heckl1988]*. If the dipoles could align freely without limitations a dipoles would always be attracted toward the strongest part of an electric field. This is in fact the case for the water molecules in the subphase thereby raise the water level in the field region. The effect was only observed with the use of strong fields but negligible and had no influence on the induced area.

Electric Gradient Field - Two approximations.
The thickness of the electrode and the distance from this to the monolayer is of the same order. The thickness is 0.005" = 127μm and the distance d_0 to the monolayer is $\geq 200\mu$m. The two most straight forward approximations of the field are (1) a point charge as done by *[Mohwald1986]* or (2) a vertical charged rod *[Heckl1988]*. The charged rod is given by an integration of stacked point charges along the length of the rod. The electric gradient field across the monolayer plane z=0 is given from a point charge:

$$E_{z,Q}(r) = -\frac{\partial \Psi(r,z)}{\partial z}|_{z=0} = -const\frac{2d_0}{(r^2+d_0^2)^{\frac{3}{2}}} \tag{6.5}$$

Integrating along the length of the electrode l from d_0 to $d_0 + l$ gives the field from a line charge:

$$E_{z,Rod}(r) = \int_{d_0}^{d_0+l} E_{z,Q}(r)dd_0 = const'\left(\frac{1}{(r^2+(l+d_0)^2)^{\frac{1}{2}}} - \frac{1}{(r^2+d_0)^{\frac{1}{2}}}\right) \tag{6.6}$$

The second term in eq. (6.6) is now neglected since $l \ll d_0$. The two constants includes the charge Q and the capacity of the system depending on the geometries of the electrode and are thus different. The field from a point charge and a solid sphere are equal so $const \approx bU$, where $b = 63.5\mu$m is the radius of the sphere (i.e. the electrode). For the thin rod $const' \approx U$.

Force on the Domains in the Field.

$$F_{r,Q}(r) = p_z\frac{\partial E_z}{\partial r} = p_z const\frac{6d_0 r}{(r^2+d_0)^{\frac{5}{2}}} \tag{6.7}$$

$$F_{r,Rod}(r) = p_z\frac{\partial E_z}{\partial r} = p_z const'\frac{r}{(r^2+d_0)^{\frac{3}{2}}} \tag{6.8}$$

Solutions for both the electric fields and forces are plotted in *fig. 6.14* for voltages of $300, 200, 100V$ with $d_0 = 200\mu m$.

Energy Considerations of the Field-Dipole interaction.
At room temperature the thermal energy given by k_BT is of the order of $1 \cdot 10^{-21}$J. The energy of one dipole with dipole moment 0.5Debye aligned to an electric field of strength 10^6V/m is $G = \mathbf{p} \cdot \mathbf{E} = 1.7 \cdot 10^{-24}$J. Thus in the strongest part of the field beneath the electrode the thermal energy exceeds the energy of a single DPPC molecule.

For the situation with a domain of radius a in the electric gradient field the energy is given by an integral of the field over all dipoles contained in the domain. For simplicity the domain is situated at the center of the field r=0:

$$G = \int_0^a \int_0^{2\pi} r\overline{p}E_z(r)drd\phi \tag{6.9}$$

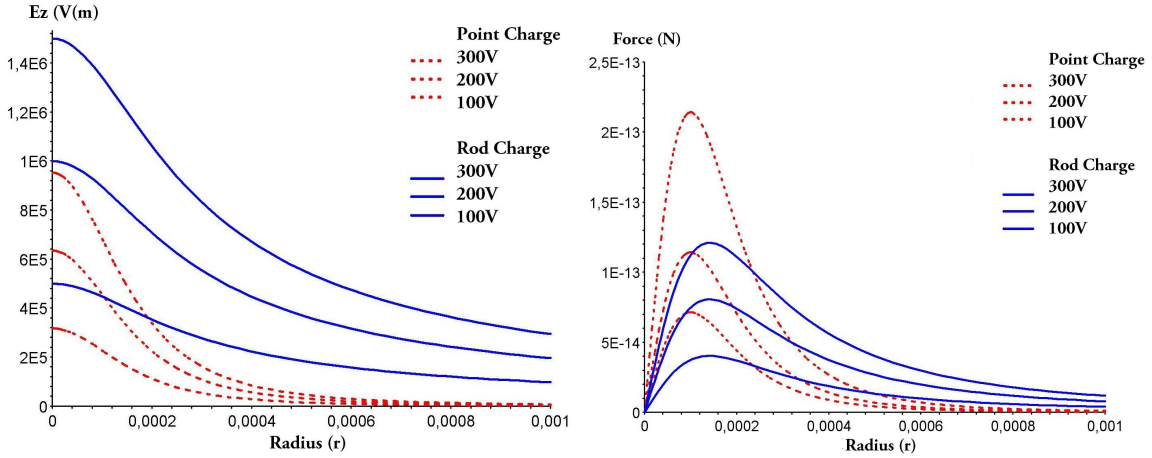

Fig. 6.14: Solutions with U = -300V,-200V,-100V of the electric field. ***Left:*** *For both a point charge and a rod charge approximation.* ***Right:*** *The force acting on a domain is the positive moving forcing domains away from r=0. The distance from charge to monolayer $d_0 = 200\mu$m. The dipole moment density of the lipids in the domain is assumed to be 0.5Debye/49Å^2 and domain radius 10μm.*

Calculation of G using the rod approximation $E_{z,Rod}(r)$ gives:

$$G_{Rod} = \int_0^a \int_0^{2\pi} r\overline{p}E_{z,Rod}(r)drd\phi = 2\pi\overline{p}U\left(-\sqrt{a^2+d_0^2}+d_0\right) \tag{6.10}$$

For the case with the point charge the energy is given *[Mohwald1986]* as:

$$G_Q = \int_0^a \int_0^{2\pi} r\overline{p}E_{z,Q}(r)drd\phi = 4\pi\overline{p}d_0bU\left(\frac{1}{\sqrt{a^2+d_0^2}}-\frac{1}{d_0}\right) \tag{6.11}$$

In the case of attraction U=300V, $d_0 = 200\mu$m the energy G of a domain of radius $a = 10\mu$m centered at r=0 can be calculated using eq. (6.11) and (6.10) yields respectively $1\cdot10^{-15}$J and $1.6\cdot10^{-15}$J. Both energies are larger than the thermal energy by a factor of 10^6 clearly shows the favorable centered position of the domain in the field.

It is worthwhile to calculate the repulsive force F_{rep} and the related energy W_{rep} of a domain-domain interaction in the monolayer in presence of the electric gradient field. Assume that the two domains are equal with the above used parameters $a = 10\mu$m and $\overline{p} = 0.5$Debye/49Å^2. The electric field of a surface normal dipole $\mathbf{p}_1$ at a point $\mathbf{r}$ is given *[Griffiths1999]*:

$$\mathbf{E}_{dip} = \frac{1}{4\pi\epsilon_0 r'^3}(3(\mathbf{p}_1\cdot\mathbf{r})\mathbf{r}-\mathbf{p}_1) \tag{6.12}$$

In the monolayer plane $\mathbf{p}_1\cdot\mathbf{r} = 0$.

Thus the radial component of the force $\mathbf{p}_1$ exerted on the other dipole $\mathbf{p}_2$ a distance r' away is derived with eq. (6.4):

$$\mathbf{F}_{1,2} = \frac{3\mathbf{p}_1\mathbf{p}_2}{4\pi\epsilon_0 r'^4}\mathbf{r} \tag{6.13}$$

Now having the two dipoles equal $\mathbf{p}_1 = \mathbf{p}_2$ the energy W it takes to move $\mathbf{p}_2$ from ∞ to a distance r' toward $\mathbf{p}_1$ is:

$$W_{rep} = \int_{\infty}^{r'} \mathbf{F}_{1,2} dr' = \frac{p^2}{4\pi\epsilon_0 r'^3} \tag{6.14}$$

With the shortest possible distance between the domains as 2 times the radius $r' = 2a$, F_{rep} and W_{rep} are respectively $9.4 \cdot 10^{-14}$N and $1.3 \cdot 10^{-19}$J. These indicate that dense packing of domains are possible in presence of the approximated electric gradient fields.

6.6 Conclusion

An experimental setup has been designed and constructed for electrical manipulation of monolayers with an electrical gradient field. Drift in the monolayer and evaporation of the subphase were avoided with the setup. This is fulfilled by an experimental protocol and user guide.

Successful manipulation of DPPC monolayers was carried out with the final setup. This includes attraction and repulsion of domains in the monolayer enabling the measurements of the applied voltage and size of induced area. The relation of applied voltage and induced area is found to be a power law $R_0^2 = 100\frac{\mu m^2}{V}U$. This is valid for both an induced domain cluster and a induced domain free area.

Repulsion and attraction caused by the electric gradient field proves the dipole behavior of condensed DPPC domains in a monolayer. The direction of these movements agrees with those predicted by electrodynamic laws with correct signs. A dielectric behavior of the monolayer that only causes attraction of the domains into the strongest part of the applied field is not observed. The liquid phase of the monolayer was not observed to be affected by the field.

Condensed domains were observed to reorient and have a preferred orientation in the field which implies an inhomogeneous distribution of the dipoles in DPPC domains.

The models outlined the strong dependence on the vertical component of the dipole moment but an equilibration radius of the induced area could not be estimated from these. Experiments and the two approximations agree in fundamentals however an exact calculation of the force exerted on the domains is not a part of this thesis. Energy calculations with the model show the possibility of the experimental observations. In presence of the electric gradient field it can be stated that the energy of a single DPPC lipid is of the order $G = 1.75 \cdot 10^{-24}$J. At the temperatures used this energy of a single dipole in the field is much lower than the thermal energy which is of the order of $k_B T = 1 \cdot 10^{-21}$J. By this, single molecular order induced by the applied field is disabled. The story is different for the condensed domains which carry an more or less in-frozen dipole moment. The energy of a single domain of radius 10μm in the center of the approximated fields is of the order $G_{Rod} \approx G_Q = 1 \cdot 10^{-15}$J. Compare this energy to the energy of two similar domains of the

order $W_{rep} = 1.3 \cdot 10^{-19}$J, a dense domain packing is possible in the center of the field. Condensation or fusion of domains are not observed in any case. It can then be stated experimentally and theoretically that in the region of coexistence, a local phase transition between (LE) and (LC) can be induced in the local gradient field region.

Chapter 7

Summary & Outlook

7.1 Summary

The work presented in this thesis concentrates on the morphology and electrical manipulation of the coexistence region of DPPC monolayers. DPPC has been chosen because of its representation in a variety of cell membranes and its excellence as a monolayer model for membranes at room temperature. Furthermore, it is one of the most studied phospholipids in literature. Information was obtained with the use of a designed setup for electric stimulation and the existing technique of a Langmuir trough and Wide field Fluorescence Microscopy.

The following experimental results are achieved.

- It is shown with the use of DSC measurements that TRITC-DHPE in amounts of 0.2mol% and 0.4mol% has no influence on the melting properties of hydrated multi lamellar vesicles. Neither the melting temperature nor the width of the melting transition is affected.

- The powerful combined technique of a WFM and a Langmuir through is used to visualize and confirm the morphology of DPPC monolayers on a subphase of 150mM NaCl with an emphasize on the (LE-LC) coexistence region. In this region the condensed lipid domains mostly develop a bean shape but also lobed and oddly shaped domains appear. Isotherms for different temperatures of DPPC monolayers are obtained expressing phases and transitions to a fine degree with a dependency on temperature comparable with literature.

- A setup for the electric gradient field is build to fit into the existing Langmuir-WFM setup. This is used to confirm the results from the Möhwald group. It is found that a positive charged top electrode causes attraction of condensed lipid domains in the (LE-LC) region while a negative charged electrode causes repulsion. In both cases a circular area is created of either condensed domains or empty of domains. These areas are found to grow with the duration time of the field with a decreasing rate of growth. To quantify the influence of the electrical field on the DPPC monolayer an equilibrium

radius R_0 of the areas is defined. For the used geometry of the top electrode the dependency of the areas affected on the applied voltage U is within errors, found to follow $R_0^2 = 100\frac{\mu m^2}{V}U$ which agrees with the result previously obtained by *[Heckl1988]* for a different electrode geometry.

Condensed domains were observed to reorient and have a preferred orientation in the field which implies an inhomogeneous distribution of the dipoles in DPPC domains. See also *[Florsheimer1989]*.

Theoretically estimations of energies show that dense domain packing in the electric gradient field is possible which agrees with similar estimations by *[Mohwald1986]*. The state of a single lipid in the liquid expanded phase in the field region is dominated by thermal motions. The more or less non-interaction of the headgroup agrees with the free orientation the headgroup which was indicated by melting enthalpy data of (PCs). This agrees with the observations of field induced movement of domains and that the liquid expanded phase is unaffected by the field.

It can then be stated experimentally and theoretically that in the region of coexistence, a local phase transition between (LE) and (LC) can be induced in the local gradient field region.

The following experiments are performed but not proceeded.

★ The experiments with a homogeneous electric field applied across a DPPC monolayer only show a week effect on the monolayer and no attraction or repulsion of domains. Such effect must be influenced by the homogeneous field, the fringing field (boundary field) and the drastic rise of the water level. For these reasons it was terminated but the raise in water level h iss found to obey $h \propto U^2$ as in general for dielectrica. Appendix A.1.

★ Direct stimulation of DPPC a monolayer with an AC current between two electrodes separated by 2mm and detection with a capacitor like setup was also carried out. This looked promising for a detection of a possible propagating density wave in the monolayer because the dipole potential of a DPPC monolayer depends on its state. The detected signals were found to be simultaneous with the stimuli. The magnitude of the signal increased during the formation of the (LE) phase and at higher values of the lateral pressure a saturation in the signal was reached. For different reasons this was not reproducible, see Appendix A.2.

All in all the fluorescence method for imaging monolayers combined with a electric gradient field emphasize the role of the polar head groups of DPPC. A similar influence of a gradient electric field on a variety of lipids with polar head groups reported in literature[1] highly indicates that the state of a cell membrane containing zwitterionic lipids can

[1]DLPE, DMPE and DMPA at pH 11 *[Mohwald1986]*, DPPC *[Heckl1988]*, the mixtures (DMPC:DSPC), (DLPC:DSPC) and (Sm:Cer) *[Wilke2006a]*

be locally changed in the field region. The question of inspiration for the experimental work in this thesis *"How does electrical stimulation of a nerve affect the main membrane components - the lipids?"* is actually of relevance.

7.2 Outlook

To provide a deeper understanding of the coupling between an electric gradient field and a monolayer, the effect (induced areas) has to be measured at different lateral pressures at a constant temperature. Since only the domains are affected, the coexistence region is of interest and the results should obviously be correlated with compressibility of the monolayer.

In the case of repulsion, the effect is expected to decreases toward the transition to the pure (LC) phase but increases toward the transition to the (LE).

For the case of attraction, the expectation is reversed. The two effects will then be equal at the point where the monolayer is covered by an equal amount of domains and liquid expanded phase.

Conclusive information of the dipole moment of the headgroups of DPPC can be drawn if an applied gradient electric field on a monolayer consisting of negative charged lipid DPPG shows no effect. Thus intuitively, the negative charges only feel a force directed opposite to the electrical field. However, if only attraction of DPPG domains occur for both directions of the field, an induced dipole moment in the lipids must be stated.

7.2.1 Experimental Extensions

The setup for the gradient field presented in this work suffers from the lack of visualizing the whole area affected by the field in one image. To achieve this one should use an objective of lower magnification (5x or 10x) that has a large working distance which is necessary for location of the top electrode. A disadvantage of such an objective is observation of smal changes of the domain shapes.

Estimation of the force of the gradient field is only able if the top electrode used has a genuine geometry that allows a "correct" approximation. Instead of a top electrode, an insulated thin wire sticking through the monolayer could be used which allows a numerical calculation of the force with Bessel functions, see *[McConnel1995]*. In that case the reduction of he field caused by the insulating material has to be calibrated.

7.2.2 Bilayer Systems

In general bilayers resemble cell membranes better than monolayers do and an extension of applied electrical fields to bilayers is obvious. One can study planar bilayers which are often

solid supported and one can prepare vesicles and use confocal microscopy *[Feigenson1999]*. The observed electric gradient field and domain interaction in DPPC monolayer is in essence kinetic and the method for studying such an interaction in bilayers has to allow dynamics. The effects of applied electric fields across membranes have in literature focused on the gaiting of ions across biological membranes (patch-clamp) or across artificial bilayers measured with the black lipid membrane technique (BLM). A deeper understanding of the mechanics of a membrane consisting of lipids with polar headgroups is not available. However, measurements of bending modulus of lipid membranes show a maximum at the melting temperature and a decrease outside the melting transition, see *[Marsh2006]*. Both a gradient and a homogeneous field might induce a bending of a membrane if it is in a state with two coexisting phases, solid ordered and liquid disordered. The experimental observation of an in-frozen dipole moment in the gel domains and the unaffected liquid phase is used to sketch such induced bending in *fig. 7.1*. A homogeneous electric field across the bilayer simply forces the gel domains (the dipoles) in direction of the field lines and induces a bending of the membrane. Similar to the monolayer experiment, a gradient field attracts the gel domains e.g on the lower leaflet toward the strongest part of the field and repels these on the upper leaflet. The degree of bending (radius of curvature) depends on the voltage applied. Thus, for a electric field on the order of the membrane field of the order 100mV/5nm = $2{\cdot}10^7$V/m a dramatic bending is expected.

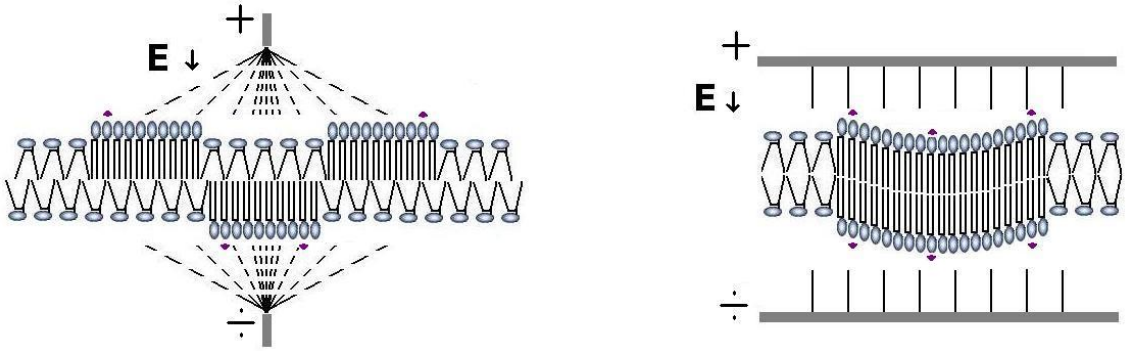

Fig. 7.1: The idea of the in-frozen dipole moments of the gel domains as found in the DPPC monolayer studies are here transfered to bilayers. These are made of e.g. DLPC:DPPC at a ratio of 67:33 which are known to form two coexisting phases, a liquid disordered and a solid ordered. Possible effects of an applied down warded electrical field ***E*** *is sketched for a gradient and a homogeneous field. The directions of the in-frozen dipole moments are indicated.* ***left:*** *The gradient field is parallel to the ordered dipoles of the lower leaflet and force these toward the center of the field similar to the effect observed with monolayers. The direction of the dipoles in the upper leaflet is antiparallel to the field and the domains with an in-frozen dipole moment are repelled from the center of the field.* ***right:*** *A homogeneous field is applied across the bilayer. In this case the force on the dipoles is not a gradient force but the in-frozen dipoles are forced in the direction of the field. This system is similar that of a black lipid membrane where the ionic media on both sides of the membrane acts as conducting plates. In both of the sketched cases a bending of the membrane is possible. The degree of bending (radius of curvature) has to depend on the voltage applied.*

Appendix A

A.1 Effect of Homogeneous Field.

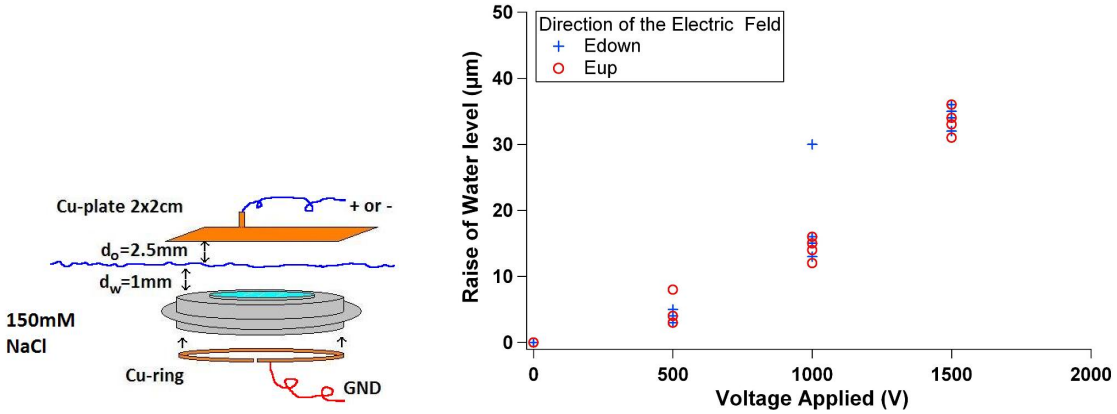

Fig. A.1: ***Left:*** *Schematic of experimental setup for homogeneous* ***E*** *field across a monolayer. At the boundaries the field is a gradient field (fringing field) .* ***Right:*** *Attraction of dielectric water and raise of water level.*

Effects of a homogeneous electric field applied across DPPC monolayers were investigated with a setup sketched in *fig. A.1 left*. The field was produced between the $150mM$ NaCl subphase and a $2 \times 2cm$ Cu plate $2.5mm$ above monolayer. Parallel or anti parallel aligning of the dipoles in the monolayer to the field was thought change the electrostatic repulsion between the polar molecules. Such might influence domain shapes and repulsive forces between domains.

Before fields wee applied monolayers were compressed into and a lateral pressure of $4.5N/m$ at a temperature 0f 21^oC. Normal developed domains were mostly observed. Applied Voltages to the Cu plate and the grounded subphase were of magnitudes $p \pm 500, 100, 1500V$ resulting in field strengths of the order $10^5V/m$.

Movements of domains were not observed in any cases. For very long time durations of the field, small changes in the distribution of domain were observed but only in one experiments. What was alway observed was a significant raise of the water level of several microns depending on the voltage applied but independent on the field direction *fig. A.1*

right. This was also the case with a monolayer spread. Thus, the effect is explained by the inhomogeneous field at the boundaries of the field affecting the subphase which have a dielectric behavior even in presence of sodium and chloride ions. It is then comparable to the attractive force on a dielectrica between two capacitor plates for which $F \propto V^2$.

The rarely observed change of the monolayer cannot be interpreted as a single effect but are influenced by the homogeneous field, the inhomogeneous boundary field, the rise of the water level. However freely aligning of the water molecules is demonstrated which is in contrast to the in frozen dipole moment of lipid domains observed in this work.

A.2 Direct Stimulation of DPPC Monolayers

Direct stimulation of DPPC a monolayer on 150mM NaCl with an AC current between two electrodes of silver separated by 2mm and detection with two plates on each side of the monolayer, see *fig. A.2*. the voltage difference was measured between these two plates. It would then be possible to measure a build up of charges of the plates is then caused by density wave that passes the between the plates. Stimulus was performed for 50 micro seconds: with (0, 0.2, 0.5, 1, 2, and 20mA) at different values of the lateral pressure (2, 3, 4, 5, 6, 8, 10 and 31mN/m). In the last runs (lowest pressure about 2mN/m) the stimulation signal is only detected at and above 2mA, and not at 1mA. Data presented in *fig. A.3* are all original data (i.e. non-modified) from Scope and no background subtraction has been performed. The reading time was about 60ms which was followed by an 10ms equilibration period. The curves are averages of 1024 stimuli-recordings.

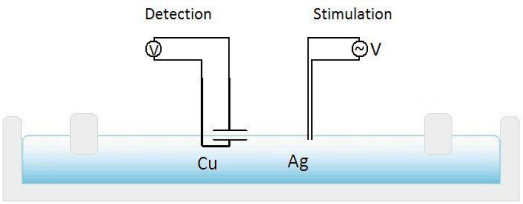

Fig. A.2: Flat Cu electrodes, c:a 0.5 x 0.5 cm (squared) were used for detection. The minus-pole electrode was placed ca 0.5-1 mm under the water surface, the plus pole (red) was placed ca 1 mm up above the interfase. These were on a lack-isolated Cu-wire (soldered to the plates).

The detected signals were found to be simultaneous with the stimuli. The magnitude of the signal increased during the formation of the (LE) phase. At higher values of the lateral pressure a saturation in the signal was reached. Note also that a stronger stimuli were needed to detect a signal at lateral pressures in the (LE) phase. For different reasons this was not reproducible. Measurements of the conductivity in both DPPC monolayers and subphases neverthe less indicates an influence by the monolayer-water interface, see *[Morgan1991]* and related work.

Note on pressure. Because of primitive experimental setup, we had some evaporation and unstable temperature over the long time of sample collection. For these reasons, the pressure determination may be inaccurate.

Technicalities:
Sample and setup description: DPPC (4mg) was dissolved in 4mL of Chloroform/Methanol (1:10 v/v%) at RT to give a 1mg/ml DPPC Stock solution.

Flat Cu electrodes, c:a 0.5 x 0.5 cm (squared) were used for detection. The minus-pole electrode was placed ca 0.5-1 mm under the water surface, the plus pole (red) was placed ca 1 mm up above the interfase. These were on a lack-isolated Cu-wire (soldered to the plates). A grounding wire (Cu as well) was arranged for, by a connection to the water phase (at the one end and to the grounded shielding of the detection Cu electrodes at the other end). The distance between the two stimulus electrodes was c:a 0.5 cm. The distence between the stimulus electrodes and sensor electrodes was c:a 3-4 cm The electrodes were located in the middle of tray, in a perpendicular direction to the tray, and the two tray-pressure-lurgs! Data recordings were arranges to provide averages of 1024 readings (sweeps) per stimulis strength (provided in mA below). Data was collected at different pressure (in a direction from high pressure to low, after having recorded a phase diagram from low P to high P.

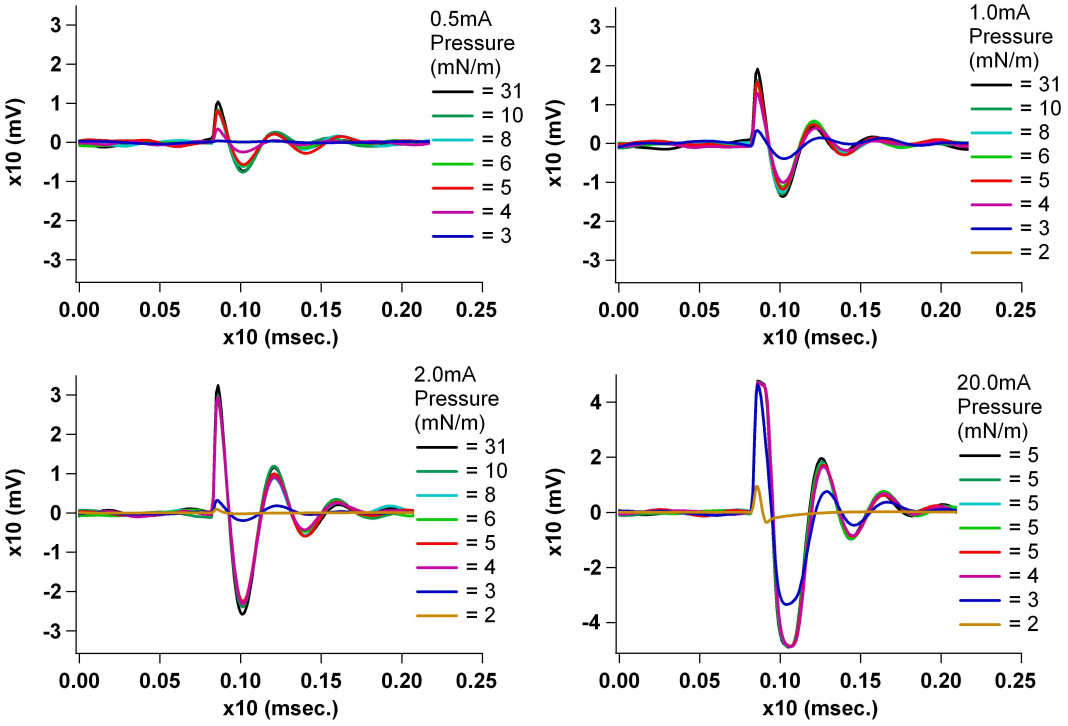

Fig. A.3: Sketch of the .

DirStimulation/DirStim0x5mA.jpg

A.3 Recipe for Trough Handling

Profound rinse of a dirty trough.
Store the trough in tap water and the soap Deconex 10% at least over night.
Rubbing with acetone, Ethanol and water until visible dirt is removed.

Sonicate in Ethanol 10% for 2x 15 minutes and rinse trough in MQ water.
Sonicate in MQ water for 10-15 minutes and sonicate inn Ethanol (99,9%) f6r 15 minutes.
Sonicate in MQ water for 5 minutes and rinse in MQ water.
Finnish with compleely drying with N_2.

Normally rinse of trough before experiment
Flush the trough under hot tap water for 15 minutes to remove dust and enlarge the trough and then lower the steel ring with the coverglass into the trough used for microscopy.
To remove agrigated lipids and substances rub the trough and especially the corners and branches with Methanol and be careful not to touch the coverglass.
Rinse totally with Ethanol (99,9%) and use MQ water for the final rinse. Use N_2 for drying.
Very important: no Ethanol must be left in the trough, else it would mix with the ssubphase.

Clean the needle for the tensiometer by flushing with ethanol on the tip which will be in contact with the monolayer and subphase. Finnish with MQ water and dry with N_2.
Use a gas burner to heat the tip until the flame is normal blue. NOTE that an exponentially drop in pressure is often caused by evaporation of water from this needle if is's not dry.

A.4 Glue a coverglass onto the steel ring

Remove old broken glass with a steel scraper. The glue used is extremely hard.

The laze way:
Store the ring with glass in acetone in a enclosed container over night in the fume cupboard...

The hard way:
Store the ring with glass in acetone and a thorough sonication has to be done with the powerfull sonicater for 15 minutes...

...Continued:
Use a steel scraper to dredge the rest of the glass and rub with Acetone to remove glass dust. (If not all glass has been removed repeat the sonicating and rubbing once more).
When all glass is removed use a fine sand paper to make the steel a little rough to increase the effect of the glue.
A finish rinse before gluing has to bee done with Acetone and Ethanol and totally drying.
Carefulness has to be taken under the gluing process if a successful result should be reached.
I.e. no glue or fingerprints on the covergass or on the rest of the steel ring.

A clean coverglass has to be prepared before gluing.
Put a narrow strobe of glue on the steel ring. Use only a very small amount! Heat the ring to $30°C$ which will make the glue homogeneous.
Place the clean coverglass on the steel ring. (There is only one try).
Harden the glue in UV light for 2 fours and 2 hours with the bottom up.
After that small amounts of Acetone has to be used to remove extra glue which else would mix with the subphase. Dry completely with N_2.
The glue has to solidify for 4-5 days at room temperature.

A.5 Locating the top electrode

The subphase used is here named water.
The WD of the x40 air objective is 2.5mm which make it suitable for focusing above the water level.
1) Focus on the cover glass in the trough using the backward reflected beam and move the trough down $200\mu m$.
2) Place the holder with the Pt electrode in the subphase behind the barrier.
3) Clean the water surface as usual leaving the barriers at the outer position and suck a little more water of than the $200\mu m$ water level.
4) Place the electrode and holder away from the focus area and ensure the electrode don't come into touch with the water.
5) Connect the electrode and adjust the hight of the electrode by lowering it until a reflection can be seen in the water. NOT further.
6) Move the holder with the electrode side wise into focus so the laser beam illuminates the electrode tip and use the acrylic cover box.
7) Move the trough further down by $250\mu m$ and locate the tip by moving the focus horizontally. Focusing is done like in 1). A nearly round spot is seen when the tip is in focus.
8) Focus vertically and you have the distance from the electrode tip to the cover glass. Check the water level. Small amounts of water can be added.

Bibliography

[Abbott1960] B. C. Abbott. Heat production in nerve and electric organs. *J. og Gen. Physiol.*, pages 119 – 127, 1960.

[Antonov1980] V. E. Antonov, A. A. Petrov, V. V. andMolnar, D. A. Predvoditelev, and A. S. Ivanov. The appearence of single-ion channels in unmodified lipid bilayer membranes at the phase transition temperature. *Nature*, 283:585 – 588, 1980.

[Benvegnu1992] D. J. Benvegnu and H. McConnell. Line tension between liquid domains in lipid monolayer. *J. Phys. Chem.*, 96:6820 – 6840, 1992.

[Biltonen1993] R. Biltonen and D. Lichtenberg. The use of differential scanning calorimetry as a tool to characterize liposome preperations. *Chemistry and Physics of Lipids*, 64:129 – 142, 1993.

[Blodgett1934] K. B. Blodgett. *J. Amer. Chem. Soc.*, 56:495, 1934.

[Brockman1994] H Brockman. Dipole potential of lipid membranes. *Chemistry and Physics of Lipids*, 73:57–79, 1994.

[Clarke2001] R. J. Clarke. The dipole otential of phospolipid membranes and methods for its detection. *Adwances in Colloid Interface Science*, 89-90:263 – 281, 2001.

[Davies1955] J. T. Davies and E. Ridael. Interfacial potentials. *Can. J. Chem.*, 33:947 – 960, 1955.

[Demchak1974] R. J. Demchak and T. Fort. Surface dipole moments of close-packed inionized monolayers at the air-water interface. *J. Colloid Interface Sci.*, 46:191 – 2002, 1974.

[Discher2002] B. M. Discher, K. M. Maloney, D. W. Grainger, and S. B. Hall. Effect og neutral lipids on coexisting phases in monolayers of pulmonary surfactant. *Biophys. Chem.*, 101-102:333 – 345, 2002.

[Feigenson1999] G. W. Feigenson, J. Korlach, P. Schwille, and W. W. Webb. Characterization of lipid bilayer phases by confocal microscopy and fluorescence correlation spectroscopy. *Proc. Natl. Acad. Sci.*, 96:8461 – 8466, 1999.

[Flewelling1986] R. F. Flewelling and W. L. Hubbell. Hydrophobic ion interactions with membranes. thermodynamic analysis of tetraphenylphosphonium binding to vesicles. *Biophys. J.*, 49:531 – 540, 1986.

[Florsheimer1989] M. Flörsheimer and H. Möhwald. Development of equilibrium domain shapes in phosholipid monolayers. *Chem. and Phys. of Lipids*, 49:231 – 241, 1989.

[Florsheimer1990] M. Flörsheimer and H. Möhwald. Growth of large liquid crystaline domains of phospholipids at air-water interface. *Thin Solid Films*, 189:379 – 387, 1990.

[Franks1976] N. P. Franks. Structural analysis of hydrated egg lectidin and cholesterol bilayers i. x-ray diffraction. *J. Mol. Biol.*, 100:345 – 358, 1976.

[Gaines1966] Geroge L. Gaines. *Insoluble Monolayers At Liquid-Gas Interface*. Interscience Publishers, John Wiley & Sons, Inc., 1966.

[Gennis1989] R. B. Gennis. *Biomembranes. Molecular Structure and Function.* Springer, 1989.

[Griffiths1999] David. J. Griffiths. *Introduction to Electrodynamics*. Prentice Hall, 1999.

[Hardy2006] N. J. Hardy, T. H. Richardson, and F. Grunfeld. Minimising monolayer collapse on langmuir troughs. *Colloids and Surfaces A*, 284-285:202 – 206, 2006.

[Hauser1981] H. Hauser, r I Pasche, Pearson R. E., and l S. Sundel. Prefered conformation and molecular packing of phosphatidylethanolamine and phosphatidylcholine. *Biochemica et Biophysica Acta*, 650:21–51, 1981.

[Hazel1979] J. R. Hazel. Influence of thermal acclimation on membrane lipid composition of rainbow trout liver. *Am. J. Physiol.*, 287:633 – 641, 1979.

[Heckl1988] W. M. Heckl, A. Miller, and H. Möhwald. Electric-field-induced domains movement in phospholipid monolayers. *Thin Solid Films*, 159:125 – 132, 1988.

[Heimburg1998] T. Heimburg. Mechanical aspects of membrane thermodynamics. estimation of the mechanical properties of lipid membranes close to the chain melting transition from calorimetry. *Biochem. Biophys. Acta*, 1415:147 – 162, 1998.

[Heimburg2005] T. Heimburg and A. D. Jackson. On soliton propagation in biomembranes and nerves. *Proc. Natl. Acad. Sci.*, 102:9790 – 9795, 2005.

[Heimburg2007] T. Heimburg. *Thermal Biophysics of Membranes*. WILEY-VCH, 2007.

[Hodgkin1952] A. Hodgkin and A. Huxley. A quantitative description of membrane current and its application to conduction and excitation in nerve. *J. of Physiology*, 117:500 – 544, 1952.

[Kandel2000] E. R. Kandel, J. H. Sxcwartz, and T. M. Jesseull. *Principles Of Neural Science*. McGraw-Hill, 2000.

[Kjaer1987] K. Kjaer, J. Als-Nielsen, C. A. Helm, L. A. Lauxhuber, and Möhwald. Ordering in lipid monolayers studied by synchrotron x-ray diffraction and florescence microscopy. *Phys. Rev. Lett.*, 58:2224, 1987.

[Kroon1989] A. I. P. M. de Kroon, J. de Gier, and B. de Kruijff. Association of synthetic model peptides with phosphalipid vesicles induced by a membrane potential. *Biochem. Biophys. Acta*, 981:371 – 373, 1989.

[Langmuir1917] I. Langmuir. The construction and fundamental properties of solids and liquids part ii liquids. *J. Am. Chem. Soc*, 39:1848, 1917.

[Loesche1984] M. Lösche and H. Möhwald. Inverted fluorescence microscopy. *Rev. Sci. Instrum.*, 55:1968, 1984.

[Losche1983] M. Lösche, E. Sackmann, and H. Möhwald. A fluorescence microscopic study concerning the phase-diagram of phospholipids. *Ber. Busenges. Phys. Chem.*, 87:848 – 852, 1983.

[Marsh2006] D. Marsh. Elastic curvature constants of lipid monolayers and bilayers. *Chem. and Phys.of Lipids*, 144:146 – 159, 2006.

[McConnel1995] H. M. McConnel and K. Y. C. Lee. Effect of electric field gradients on lipid monolayer membranes. *Biophys. J.*, 68:1740 – 1751, 1995.

[McConnell1990] H. M. McConnell, P. A. Rice, and D. J. Bervegnu. Brownian motion of lipid domains in electrostatic traps in monolayers. *J. Phys. Chem.*, 94:8965 – 8968, 1990.

[McConnell1993] H. M. McConnell. Elementary theory of brownian motion of trapped domains in lipid monolayers. *Biophys. J.*, 64:577 – 580, 1993.

[Mellier1989] A. Mellier. Infared study of phospholipid hydration. new thermodynamic data about the main phase transition of saturated phosphatidylcholine water multilayers. *Chem. and Phys. of Lipids*, 51:23 – 29, 1989.

[Mohwald1986] H. Möhwald and A. Miller. Collecting two-dimensional phosphalipid crystals in inhomogeneous electric fields. *Europhys. Lett.*, 2:67 – 74, 1986.

[Mohwald1998] H. Möhwald, J. B Li, R Miller, and D. Vollhard. Spreading concentration effect on the morphology of phospholipid monolayers. *Thin Solid Films*, pages (327–329) 84–86, 1998.

[Mohwald1999] H. Möhwald, P. Dutta, and V. M Kanagar. Structure and phase transitions in langmuir monolayers. *Review of the Modern Pysics*, 71 (3), 1999.

[Morgan1991] H. Morgan, D. M. Taylor, and N. Oliveria. Proton transport at the monolayer-water interface. *Biochem.Biophys. Acta*, 1062:149 – 156, 1991.

[Mouritsen2007] O. Mouritsen, T. Bjø rnholm, and L. K. Nielsen. Thermodynamic and real-space structural evidence of a 2d critical point in phospholipid monolayers. *Langmuir*, 23:11684 – 11692, 2007.

[Nakahara2005] H. Nakahara, S. Nakamua, S. Lee, G. Sugihara, and O. Shibata. Inluence of a new amphiphili peptide with phospholipid monolayers at the air-water interface. *Colloids and Surfaces A*, 270-271:52 – 60, 2005.

[Napolitano1967] L. Napolitano, F. LeBaron, and J Scaletti. Preservation of myelin lamellar structures in the absence of lipid. *J. Cell Bio.*, 94:817 – 826, 1967.

[Neher1976] E. Neher and B. Sakmann. Single-channel currents recorded from membrane of denervated frog muscle fibers. *Nature*, 260:799 –802, 1976.

[Nyquist2002] H. Nyquist. Certain topics intelegraph transition theory. *Proceedings of the IEEE*, 90 (2):280 – 305, 2002.

[Palush2002] M. Palush. Electrical properrties of free surface of water and aqueous solutions. *Adwanced Colloid and Interface Sci.*, 84:27 – 45, 2002.

[Parfenyuk2002] V. I. Parfenyuk. Surface potential at the gas-aqueous solution interface. *Colloid J.*, 64:588 – 595, 2002.

[Pink1982] D. A. Pink and A. Georgallas. Phase transitions in monolayers of saturated lipids. exact resuts and monte carlo simulations. *J. of Colloid and Interface Sci.*, 89 (1):107 – 116, 1982.

[Pockels1891] A. Pockels. *Nature*, 43:437, 1891.

[Rayleigh1879] Rayleigh. Investigations in optics with special reference to the spectroscope. resolving or seperating power of optical instruments. *Phil. Mag.*, 8:261 – 274, 1879.

[Rayleigh1889] Rayleigh. *Philos. Mag.*, 48:321, 1889.

[Russel1975] E. J. Russel, H. Bruce, and H. C. Andersen. A theory of the chain melting phase transition of aqeous phospholipid dispersions. *Proc. Nat. Acad. Sci. USA*, 72 No. 10:3993 – 3997, 1975.

[Sackmann1995] E. Sackmann. *Physical basis of self organization and function of membranes: Physics of Vesicles.* 1995.

[Saxton1987] M. J. Saxton. Lateral diffusion in an archipelago - the distance dependence of the diffusion constant. *Biophysical Journal*, 51(2):A542–A542, 1987.

[Shapovalov1998] V. L. Shapovalov. Interaction of dppc monolayer at air-water interface with hydrophobic ions. *Thin Solid Films*, 327 - 329:599 – 602, 1998.

[Skoog1982] Douglas A. Skoog and Donald m West. *Fundamentals of Analytical Chemistry*. Saunders College Publishing, 1982.

[Tasaki1939] I Tasaki. Electric stimulation and the excitatory process in the nerve fiber. *Amer. J. Physiol.*, 125:380 – 395, 1939.

[Tasaki1980] I. Tasaki and K. Iwasa. Mechanical changes in giant axons associated with production of action potentials. *Biochem. and Biophys. Research Communications*, 95(3):1328 – 1331, 1980.

[Tasaki1989] I. Tasaki, K. Kusano, and P. M. Byrne. Rapid mechanical and thermal change in the garfish olfactory nerve associated with propagated impulse. *Biophys. J.*, 55:1033 – 1040, 1989.

[Tasaki1992] I. Tasaki and P. M. Byrne. Heat production associated witha propagated impulse in the bullfrog myelinated nerve fibers. *Jpn. J. Physiol.*, 42:805 – 813, 1992.

[Tasaki1999] I. Tasaki. Rapd structural changes in nerve fibers and cells associated with teir excitatory processes. *Jpn. J. of Physiol.*, 49:125 – 138, 1999.

[Taylor2000] D. M Taylor. Developments in the theoretical modelling an experimental measurement of the surface potential of ordered monolayers. *Adwances in Colloid and Interface Sci.*, 87:183 – 2003, 2000.

[Teissie1994] J. Teissi, N. Denocurt, and P. Tancrde. The main transition of dipalmitoylphosphatidylcholin.e monolayers: A liquid expanded to solid condensed high order transformation. *Biophys. Chem.*, 49:153 – 162, 1994.

[Vanderlick1998] T. K. Vanderlick and C. W. McConlogue. Monolayers with one components of variable solubility: Studies of lysophosphocholine/dppc mixtures. *Langmuir*, 14:6556 – 6562, 1998.

[Vogel1988] V. Vogel and D. Möbius. Local surface potentials and electric dipole moments of lipid monolayers: Contribution of the water/lipid and the lipid/air interface. *Journal of Colloid and Interface Science*, 129 (2):408 – 420, 1988.

[Volhardt2006] D. Volhardt. Nucleation in monolayers. *Advance in Colloid and Interface Science*, 123-126:173 –188, 2006.

[VonTscharner1981] V. Von Tscharner and H M. McConnell. An alternative view of phospholipid phase behavior at the air-water interface. microscope and film balance studies. *Biopfys. J.*, 36 (2):409 – 419, 1981.

[Wilke2006] N. Wilke, S. A. Dassie, E. P. M. Levia, and B. Maggio. Externally applied electric fields on immiscible lipid monolayers: Repulsion between condensed domains precludes domain migration. *Langmuir*, 22:9664 – 9670, 2006.

[Wilke2006a] N. Wilke and B. Maggio. Effect of externally applied electric fields on the surface topography of ceramide-enriched domains in mixed monolayers with sphingomyelin. *Biophys. Chem.*, 122:36 – 42, 2006.